Journal of
Medicinal Chemistry

Article

Discovery of a Dual Tubulin Polymerization and Cell Division Cycle 20 Homologue Inhibitor via Structural Modification on Apcin

Pan Huang, Xiangyang Le, Fei Huang, Jie Yang, Haofeng Yang, Junlong Ma, Gaoyun Hu, Qianbin Li, and Zhuo Chen

J. Med. Chem., **Just Accepted Manuscript** • DOI: 10.1021/acs.jmedchem.9b02097 • Publication Date (Web): 15 Apr 2020

Just Accepted

is published by the American Chemical Society. 1155 Sixteenth Street N.W., Washington, DC 20036

Discovery of a Dual Tubulin Polymerization and Cell Division Cycle 20 Homologue Inhibitor via Structural Modification on Apcin

Pan Huang,[†,#] Xiangyang Le, [‡,#] Fei Huang, [§] Jie Yang,[†] Haofeng Yang,[†] Junlong Ma[‖], Gaoyun Hu,[†] Qianbin Li,[†] Zhuo Chen[,†]*

[†] Department of Medicinal Chemistry, Xiangya School of Pharmaceutical Sciences, Central South University, Changsha 410013, Hunan, China

[‡] Department of Pharmacy, Yiyang Central Hospital, Yiyang 413000, Hunan, China

[§] Center for Medical Experiments, Third Xiangya Hospital of Central South University, Changsha 410013, Hunan, China

[‖] Department of Good Clinical Practice, Taihe Hospital, Hubei University of Medicine, Shiyan 442000, Hubei , China

ABSTRACT: Apcin is one of few compounds that have been previously reported as a Cdc20 specific inhibitor, although Cdc20 is a very promising drug target. We reported here the design, synthesis, and biological evaluations of 2,2,2-trichloro-1-aryl carbamate derivatives as Cdc20 inhibitors. Among these derivatives, compound **9f** was much more efficient than the positive compound apcin in inhibiting cancer cell growth, but it had approximately the same binding

affinity with apcin in SPR assays. It is possible that another mechanism of action might exist. Further evidence demonstrated that compound **9f** also inhibited tubulin polymerization, disorganized the microtubule network, and blocked the cell cycle at the M phase, with changed in the expression of cyclins. Thus, it induced apoptosis through the activation of caspase-3 and PARP. In addition, compound **9f** inhibited cell migration and invasion in a concentration-dependent manner. These results provide guidance for developing the current series as potential new anti-cancer therapeutics.

■ INTRODUCTION

Ubiquitination by the ubiquitin proteasome system (UPS), a post-translational modification, plays a critical role in regulating a plethora of cellular processes, including cell death, cell cycle progression, migration, and invasion by governing the degradation of various related proteins.[1] It is a sequential three-enzyme cascade catalyzed by activating (E1), conjugating (E2), and ligating (E3) enzymes, and notably, E3 ubiquitin ligases provide substrate specificity. Among the E3 ubiquitin ligases, emerging evidence indicates the anaphase-promoting complex/cyclosome (APC/C, a 1.5MDa ubiquitin ligase comprised of 19 subunits) is the major driving force controlling the timely cell cycle process, especially in M and G1 phases.[2-4] Cell division cycle 20 homologue (Cdc20) and Cdc20 homologue protein 1, Fzr1 (Cdh1), are two related but functionally distinct activators of APC/C that are also known as APC^{Cdc20} and APC^{Cdh1}, respectively. These two activator proteins regulate the ubiquitin-mediated degradation of specific substrates, thus promoting the cell cycle forward in a unidirectional manner.[5] Cdc20 activates the APC/C during early mitosis, while Cdh1 associates with the APC/C during late mitosis and

extends into the G1 phase. Notably, it has been demonstrated that Cdh1 is a tumor suppressor, while Cdc20 is an essential developmental gene.[6-8]

Cdc20 functions as an oncogenic factor in tumorigenesis, and it is overexpressed in multiple types of cancer types, including hepatocellular carcinoma, breast cancer, and ovarian cancer.[9-10] Its elevated expression correlates with shorter five-year survival, poorer prognosis, and pathological tumor status in a broad spectrum of human malignancies.[11-14] During the cell cycle, as soon as all sister chromatids are attached to the bipolar spindles, Cdc20 is released from spindle assembly checkpoint (SAC) and the formation of active APC/Cdc20 is initiated. Cdc20 binds to APC/C, induces the metaphase-anaphase transition, triggers chromosome segregation in anaphase, and ensures mitotic exit by recruiting downstream substrates for subsequent proteolysis of 26S proteasomes. Any defect in this process causes abnormal cell division. Since cell arrest at mitosis is an effective strategy to induce neoplastic cell death, Cdc20 represents a potential novel target for future cancer treatment.

Given the vital oncogenic role of Cdc20 in the development and progression of human cancers, its inhibitors could provide a therapeutic window in multiple human malignancies. Apart from the majority of small-molecule pan-APC/C inhibitors,[15-21] apcin is the only specific pharmacological inhibitor of Cdc20, which occupies the destruction-box-binding pocket of WD-40 domain, competitively prevents the recognition of substrates, and disrupts PPIs (protein-protein interactions) within the Cdc20-substrate complex.[22] However, insufficient cytotoxicity against cancer cells leads to the critical disadvantage of apcin. A recent study reported that the combination of the APC/C inhibitor with paclitaxel could synergistically inhibit APC/C^{Cdc20} and microtubule dynamics, and it might represent a new strategy to improve anti-cancer efficacy.[23-24]

Microtubules are critical drug targets in anti-cancer chemotherapy. Chemically diverse compounds interfering with microtubule dynamics are divided into two major classes: the stabilizing agents, such as taxanes, and the destabilizing agents, such as vinca alkaloid domain ligands and colchicine site ligands. Similar to APC/C-Cdc20 inhibition, microtubule interfering agent (MIA) exerts its strikingly anti-tumor effects via blocking the mitotic exit, followed by late apoptosis.[25-27] However, MIAs induce G2/M arrest by SAC activation in response to perturbations in microtubule dynamics.[28] Many cancer cells have a weakened SAC and upon protracted mitotic arrest, these cells might enter the tetraploid G1 phase state, the phenomenon of which is referred to as mitotic slippage. Background degradation of cyclin B due to residual APC/C activity is the most likely cause of mitotic slippage. These tetraploid cells either die from apoptosis in G1, entering senescence, or continue to cycling, leading to genetic instability and tumorigenesis, thus fueling tumor resistance against microtubule agents.[29] Therefore, inhibiting Cdc20 is considered to be an effective approach to overcome this side effect. Another shortcoming of MIAs is their toxicity to normal cells, while studies have reported that cancer cells are increasingly dependent on APC/C function. In general, the APC/C^{cdc20} inhibitor can enhance the sensitivity of MIAs to tumor cells. Meanwhile, MIA treatment could render tumor cells more vulnerable to APC/C inhibition. Together these findings suggest that simultaneously targeting Cdc20 and microtubules, thereby stabilizing cyclin B and preventing mitotic slippage, may be a promising therapeutic approach in cancer treatment.

In the present study, a series of Cdc20 inhibitors with the ability to inhibit microtubule function using a “two-punch strategy” (strong mitotic arrest followed by blocking mitotic exit) were synthesized.[30-31] Their in-vitro effects on HepG2 cells were evaluated and their mechanisms of action in cancer therapy were elucidated.

■ RESULTS AND DISSCUSSION

Chemistry Target compounds **5a-10c** were synthesized in a five-step procedure as described in Scheme 1. Commercially available metronidazole, phenylmethanol, ethanol, 2-pyridylethanol, 4-morpholineethanol, and (1-methyl-5-nitro-1H-imidazol-2-yl) methanol were reacted with chloroformate, and the obtained intermediates were subsequently used for the preparation of the corresponding carbamate derivatives by ammonolysis. The reaction of the amino group of the carbamate derivatives with chloral hydrate led to the formation of products that were converted quantitatively into the key intermediates **4a-f** by further chlorination. Treatment of **4a-4f** with pyrimidines, fused heteropyrimidines, and benzoylpyridines gave the desired 2,2,2-trichloro-1-aryl carbamate derivatives **5a-10c** (Schemes 2 and 3).

Scheme 1. Synthesis of Key Intermediates 4[a]

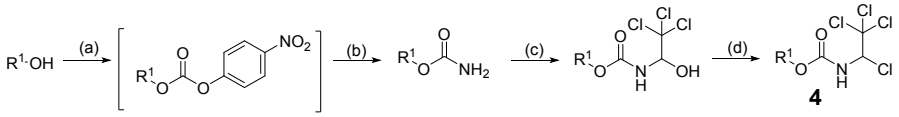

[a]Reagents and conditions: (a) Et_3N, 4-nitrophenyl chloroformate, DCM, rt, overnight; (b) $NH_3 \cdot H_2O$, DCM, 0-10℃, 3h; (c) chloral hydrate, rt-100℃,18h; (d)Et_3N, $SOCl_2$, DCM, 0℃, 15min, reflux, overnight.

Scheme 2. Synthesis of 2,2,2-trichloro-1-aryl Carbamate Derivatives 5a-8m[a]

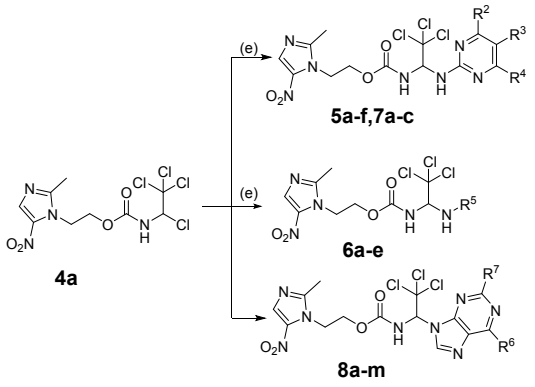

5a,R^2=R^3=R^4=H **5b**,R^2=CH_3 R^3=R^4=H
5c,R^2=OCH_3 R^3=R^4=H **5d**,R^2=OH R^3=R^4=H
5e,R^2=NH_2 R^3=R^4=H **5f**,R^2=Cl R^3=R^4=H
7a,R^2=R^4=Cl R^3=H **7b**,R^2=R^4=Cl R^3=CH_3
7c,R^2=R^4=Cl R^3=NH_2

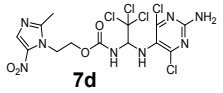

6a,R^5= **6b**,R^5= **6c**,R^5=
6d,R^5= **6e**,R^5=

8a,R^6=Cl R^7=H **8b**,R^6=dimethylamino R^7=H
8c,R^6=benzamidyl R^7=H **8d**,R^6=benzamido R^7=H
8e,R^6=NH_2 R^7=Cl **8f**,R^6=R^7=NH_2 **8g**,R^6=NH_2 R^7=F
8h,R^6=Cl R^7=NH_2 **8i**,R^6=Cl R^7=F **8j**,R^6=OBzl R^7=NH_2
8k,R^6=R^7=Cl **8l**,R^6=C=O R^7=formamido **8m**,R^6=NH_2 R^7=H

[a]Reagents and conditions: (e) aromatic amine, DCM/MeCN, rt-60℃, overnight.

Scheme 3. Synthesis of 2,2,2-trichloro-1-aryl Carbamate Derivatives 9a-10c[a]

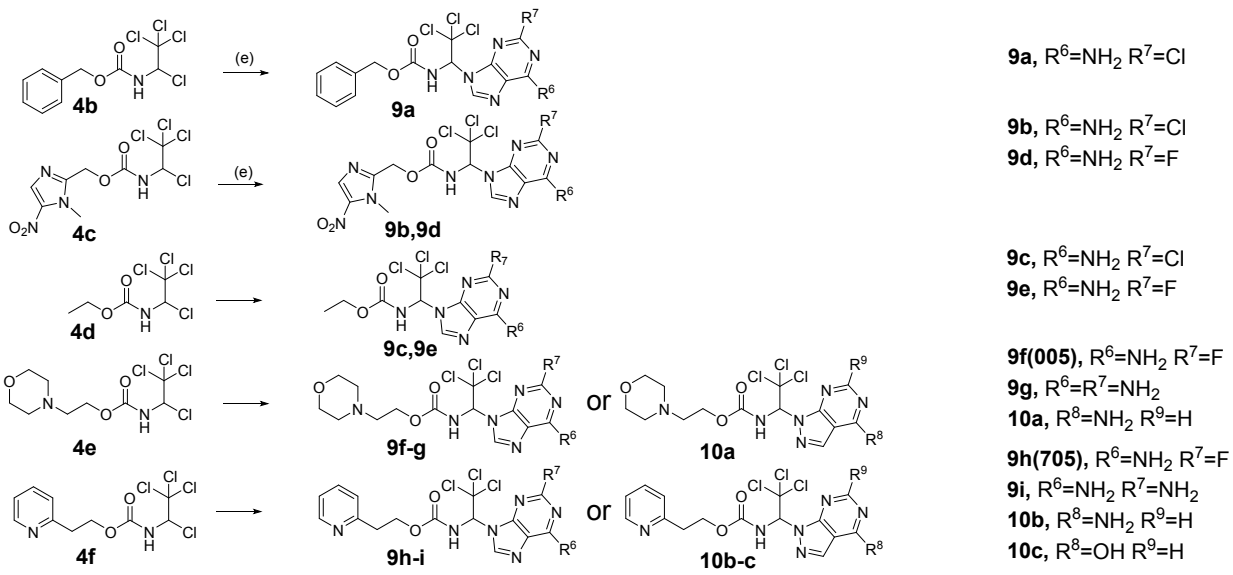

[a]Reagents and conditions: (e) aromatic amine, DCM/MeCN, rt-60℃, overnight.

In Vitro Anti-proliferative Activities and SAR Analysis In **Table 1,** the in vitro anti-proliferative activities of target compounds against a panel of seven human cancer cell lines: MCF-7 (breast cancer), A375 (melanoma), A549 (lung cancer), HepG2 (hepatocellular carcinoma), Hela (cervical cancer), Ovcar-3, and Caov-3 (ovarian cancer) were summarized using apcin as the reference compound.

Table 1. In Vitro Cell Growth Inhibitory Effects of Compounds

Cpd	IC_{50}[a], μM, ±SD						
	MCF-7	A375	A549	HepG2	Hela	Ovcar-3	Caov-3
5a(Apcin)	>300	193.3±13	>300	>300	220.8±17.9	>300	>300
5b	151.5±37.7	37.5±5.7	27.3±3.7	31.2±8.4	94.7±6.7	164.5±3.8	154.6±14.4
5c	186.0±4.4	44.1±20.2	263.8	79.8±26.8	127.6±6.2	198.3±6.7	157.4±5.6
5d	>300	>300	>300	>300	>300	>300	>300
5e	>300	>300	>300	>300	>300	>300	>300

5f	>300	20.0±9.1	94.9±10.3	>300	>300	>300	>300
6a	>300	5.3±5.1	>300	>300	>300	>300	>300
6b	99.6±2.9	14±3	47.5±25.3	22.7±2.7	9.1±0.7	90.1±4.4	72.6±20.3
6c	141.2±0.2	12.5±0.3	84.3±25.7	26.0	38.9±0.7	109.0±0.1	95.2±2.1
6d	>300	37.3±25.4	>300	46.8±5.6	>300	61.4±3.9	81.1±2.1
6e	>300	>300	>300	>300	213.9±15.9	>300	>300
7a	32.4±0.8	8.1±0.4	49.5±16.2	23.3±0.1	15.6±0.1	17.0±0.9	22.5±3.2
7b	114.0±5.6	11.9±0.5	184.3±30.9	13.6±3.1	27.1±21.0	25.0	31.2
7c	20.6±1.9	14.0±0.2	31.9±4.2	25.8±3.1	17.5±1.1	21.1±2.2	19.2±1.0
7d	159.5±5.0	34.2±1.1	56.5±2.9	25.6±6.1	63.2±0.9		109.7
8a	>300	>300	>300	>300	>300	>300	>300
8b	>300	27.3±14.1	191.3±58.2	>300	159.8±6.5	>300	264±9.3
8c	>300	>300	243.7±30.5	>300	>300	225±10.6	>300
8d	96.0±2.1	>300	148.2±47.7	33.2±16.0	71.8±8.9	243.2	>300
8e	>300	245.7±2.7	159.8±14.0	7.3±1.2	218.3±54.3	130.7±23	143.9±7.8
8f	>300	170.3±15.5	>300	19.7±3.6	120.3±1.5	>300	>300
8g	0.8	0.5±0.1	3.6±0.7	0.6	1.9±0.3	1.5±0.1	1.2
8h	>300	>300	>300	>300	57.3±3.9	>300	>300
8i	62.1±16.6	120.9±1.1	>300	55.1±13.0	>300	>300	>300
8j	89.1±54.2	>300	146.5±4.7	71.1±3.5	>300	>300	>300
8k	218.0±4.2	68.5±27.7	72.8±4.9	54.6±2.6	142.3±5.2	162±76.4	224.2±40.1
8l	>300	>300	>300	>300	>300	>300	>300
8m	>300	181.7±38.3	>300	>300	>300	>300	>300
9a	138.1±0.2	>300	78.5±1.1	>300	>300	37.9±2.6	65.0±31.7
9b	53.3±0.4	1.2±0.8	61.4±13.7	43.8±1.4	51.2±0.9	70.4±2.6	64.3±11.9
9c	87.2±34.2	125.3±92.9	59.7±6.0	59.0±11	152.0±18.5	131.7±1.6	92.9±3.9
9d	1.5±0.1	2.7±0.5	0.5±0.1	3.8±0.1	0.2	0.6±0.4	0.3±0.1
9e	0.8	1.8±0.1	0.5±0.2	1.4	0.9	0.5±0.1	0.6
9f	0.2±0.1	0.7±0.1	1.5±0.5	0.6	0.3±0.2	1.7±0.4	1.5±0.1

9g	125.4±20.8	94.7±46.4	47.2±18.1	8.6±2.1	47.5±11.9	11.5±6.7	10.5±6.0
9h	1.0±0.2	0.4±0.1	3.5±0.6	1.0	3.0±0.3	0.8±0.1	1.1±0.1
9i	135.6±112	300	270.0	28.1	219.7±90.3	30.9±11.5	29.7±4.0
10a	19.3±10.9	1.2	13.4	19.5	<10	0.8	1.0
10b	161.6±53.4	>300	53.7±14.3	81.3±11.3	109.9±37.5	>300	146.3±11.5
10c	>300	>300	>300	270.6±35	>300	>300	>300

[a]IC_{50} = compound concentration required to inhibit tumor cell proliferation by 50%. Data are expressed as the mean ± SD from the dose−response curves of at least three independent experiments.

Among the (2,2,2-trichloro-1-(pyrimidinylamino)ethyl) carbamate analogues, dichloro-substituted pyrimidine derivatives **7a-d** showed potent anti-proliferative effects against all the tested tumor cell lines. By contrast, the corresponding non-substituted derivative **6a** exhibited an inhibitory effect identical to that of apcin against most of the cell lines. Intriguingly, the activity of **6a** against the A375 cell line was noticeably improved. The substitution on the pyrimidines displayed a strong influence on activity, in general of which, electron-withdrawing substituents, such as carbonyl (**5d**) and chlorine (**5f**), showed dramatically reduced activities versus the most active compound, while the methyl-substituted analogue **5b** and methoxy-substituted analogue **5c** resulted in considerably better anti-proliferative activity against the seven tumor cell lines. On the other hand, the amino-substituted analogue **5e** led to a decrease of activity, the result was contrary to our findings. In addition, pyrimidines with bulky substituents suggested improved potency. For the compounds bearing benzoylpyridines, such as 2-aminoquinoline (**6b**), 1-aminoisoquinoline (**6c**), or 3-aminoiso quinoline (**6d**), which were larger than the unsubstituted pyrimidines, increased activities were also observed.

In the case of the fused heteropyrimidine derivatives, a superiority of the purines over the pyrimidines was observed in the tested cell lines. Among all the derivatives, the greatest activity occurred when fluorine was located at the purine moiety (**8g**, **9f** and **9h**). The insertion of a

mono-group at the C-6-position of purines generally resulted in a marked loss in anti-proliferative potency (**8a**, **8b**, **8c, 8d** and **8m** with IC_{50} >300 μM). The introduction of additional substituents into the purines contributed to the improved anti-proliferative potency. Chloro-substituted analogue **8e**, amino-substituted analogue **8f**, and fluoro-substituted analogue **8g** showed higher potency than **8m**. Likewise, chloro-substituted analogue **8k** displayed higher activity than **8a**.

Finally, we explored the effect by replacing the metronidazole with other groups. However, compounds with different replacements showed no significant changes in activity (**8e** vs **9a** vs **9b** vs **9c**; **8g** vs **9d** vs **9e** vs **9f** vs **9h**), demonstrating that metronidazole seemed to be an unnecessary pharmacophore for the anti-proliferative potency of 2,2,2-trichloro-1-aryl carbamate derivatives. Moreover, the most potent compound identified in this study was the 2-morpholinoethyl (1-(6-amino-2-fluoro-9H-purin-9-yl)-2,2,2-trichloroethyl)carbamate derivative **9f**, which was at least 1000-fold more active than the reference compound apcin among the seven cancer cell lines. The comparison of pyrazolopyrimidine analogue **10a** with **10b** clearly demonstrated, once again, that morpholine was the preferred structural element and contributed to potency.

In general, fluoro-substituted analogues exhibited the most effectively anti-proliferative activity. Moreover, dichloro-substituted pyrimidine derivatives showed moderate potency and a high structural similarity to apcin. The data obtained for seven cell lines were in agreement, except that HepG2 cells were significantly sensitive to the compounds; thus, HepG2 cells were selected for further investigation.

Studies on the Binding of Cdc20 with the Apcin Analogs To gain insights into the interactions between Cdc20 and the selected potent small molecules (**7b**, **7d**, **9f**, **8g** and **9h**), a SPR based experiment for Cdc20 was performed for subsequent evaluation. Surface plasmon resonance (SPR) is an optical biosensor detection method that measures the change in the refractive index at the surface interface that occurs during a binding event. It is used to investigate the binding efficiency, as it provides information on the affinity and kinetics of molecular interactions, and the affinity associated with the interaction may be an indicator of the binding process. The results revealed that some of the selected compounds bound reversibly to Cdc20 with clear association and dissociation phases. The relatively weak binding affinity of apcin (K_D=123 μM) was consistent with its anti-proliferative potency (**Figure 1A**). Among all the compounds, **7d** showed a 2- to 3-fold increased binding affinity (K_D=49 μM) to Cdc20 compared to apcin (**Figure 1B**), while **9f** suffered a decrease in affinity (K_D=119 μM) compared to **7d** (**Figure 1C**). Moreover, **8g** exhibited a similar binding affinity (K_D=161 μM) compared to **9f** and apcin (**Figure S1**). The association and dissociation constant of **7b** and **9h** could not be determined due to their limited solubility (**Figure 1D**).

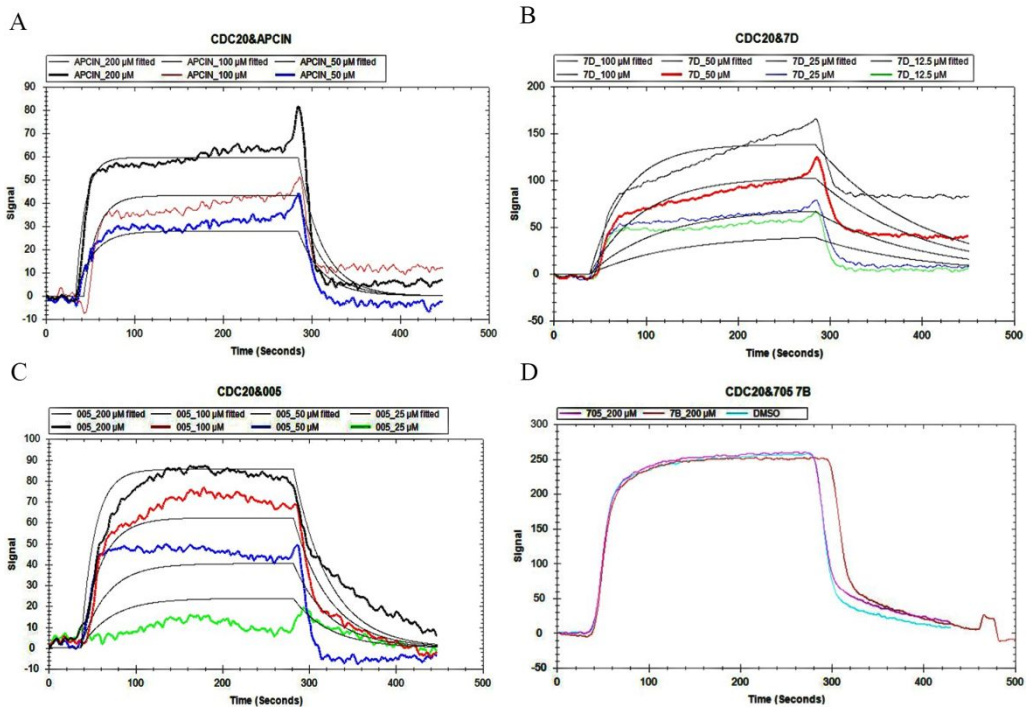

Figure 1. Sensorgrams for the interaction of (A) apcin, (B) **7d**, (C) **9f** (**005**), (D) **7b** and **9h** (**705**) with Cdc20. Molecules were tested in a dilution series starting at 200 μM. The steady state values were calculated and plotted against the concentration. A 1:1 binding model was directly fitted to the sensorgrams and a single binding site model was fitted to the data to calculate K_D.

Subsequently, compounds **7d** and **9f** were performed for a molecular modeling study, a computational tool which was previously used to determine the apcin binding site of Cdc20 as well as to elucidate the potential interactions of **7d** and **9f** with Cdc20. Overall, the overlapped 3D model revealed that **7d** and **9f**, two close analogues of apcin, were Cdc20 inhibitors, both of which bound in similar orientations to apcin and were well accommodated within the apcin site. The hydrophobic trichloromethyl groups of **7d** and **9f** were found to be buried in the pocket. However, the metronidazole, morphine, and pyrimidines groups were more peripheral. The dichloro-substituted pyrimidine of **7d** and fluorine-substituted adenine of **9f** could successfully overlap with the binding site of the non-substituted pyrimidine portion of apcin. The metronidazole moiety of **7d** and the morphine of **9f** were positioned facing the solvent.

In brief, both **7d** and **9f** underwent identical conformational changes. As for predicting the detailed molecular interactions of **7d** and **9f**, it was suggested that the phenyl ring of Tyr207 established two CH/π interactions with the linker of both **7d** and **9f** (Figures 2A and S2). The amino group of **7d** remained to form two hydrogen bonds with backbone atoms from Asp177. However, the amino group of **9f** could only form one hydrogen bond with Asp177 (Figure 2B), illustrating the higher binding affinity of **7d** with Cdc20 compared with **9f**.

The disparate conclusions between SPR studies and anti-proliferative effects prompted us to perform additional cellular or molecular biological experiments on compounds **7d** and **9f** using HepG2 cells.

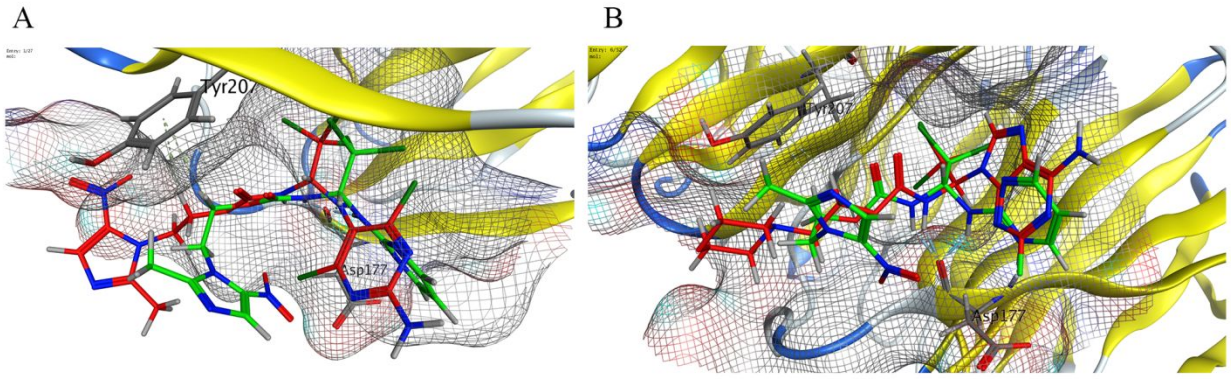

Figure 2. Predicted docking model for **7d** (A) and **9f** (B) bound to Cdc20 crystal structure (PDB ID: 4n14). Structures of **7d**, **9f** (red skeleton) and apcin (green skeleton with oxygen in red, nitrogen in blue, and proton in gray) were shown as ribbon diagrams with critical residues labeled in black and carbon atoms in gray.

7d Increased the Protein Level of Substrates Dependent of Cdc20 Rather Than Cdh1 and 9f Improved Cyclin Expression Cdc20 is critical for its ability to trigger the ubiquitination and degradation of specific substrates during the cell cycle and apoptosis. Cyclins A and B are critical for mitosis and function as substrates of both Cdc20 and Cdh1, respectively. However, cyclin B is mainly controlled by Cdc20, while cyclin A is a Cdh1 substrate. Moreover, the pro-apoptotic molecule Bim is a Cdc20 specific substrate.[32] Therefore, the influence of **7d** and **9f** on the expression of cyclin B, cyclin A and Bim were examined. The results revealed that treatment

with compound **7d** (30 μM) elevated the Bim level similarly to that in apcin-treated (100 μM) cells. Cyclins A and B were reported to regulate the mitotic cell cycle, and **7d**-treated cells showed a decrease in Cyclin B degradation (**Figure 3A**). The expression of Aurora A and Skp2 (Cdh1 specific substrates) was examined to validate the affection of **7d** to Cdh1, although there were no differences in the levels of these two proteins (**Figure 3B**). The binding affinity between **7d** and Cdc20, as well as the increase in substrates caused by **7d**, prompted us to elucidate the exact mechanism behind the delay in mitotic exit. Thus, we followed the degradation of key Cdc20 proteins, such as cyclin and Bim, in HepG2 cells. As shown in **Figure 3C**, **7d** markedly increased the stability of Bim and Cyclin B1, which peaked from 2 to 8 h, while the degradation of Aurora A significantly increased in HepG2 cells. These results reveal that **7d** (30 μM) interfered with the metaphase-to-anaphase transition and led to mitotic delay. However, treatment with **9f** (0.3 μM) seemed to have no effect on the Bim protein level, which might be due to its low concentration, but a significant increase in cyclins A and B expression was noted, indicating the efficacy of **9f** and **7d** in arresting cells in mitosis.

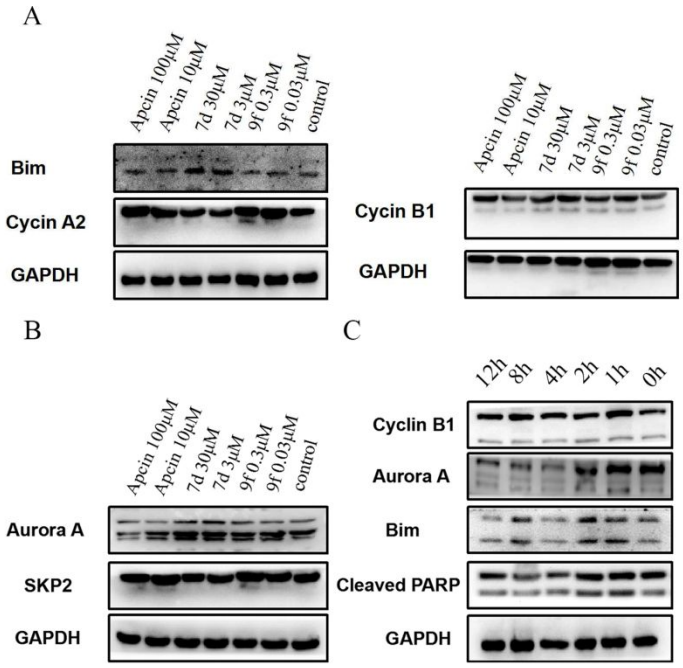

Figure 3. (A) Cdc20 substrates were analyzed to evaluate cell cycle arrest and apoptosis. Endogenous levels of PHH3, Bim, Cyclin B1 were determined. (B) Protein levels of Aurora A and SKP2 were measured by Western Blot. The results displayed that compounds had no effect on levels of Cdh1 substrates. (C) The expression of cyclin B1, Aurora A, Bim and Cleaved PARP were measured at 1 h, 2 h, 4 h, 8 h and 12 h after the addition of 30 μM **7d**.

7d and 9f Blocked Mitotic Exit in HepG2 Cells The inhibition of substrate degradation did not strictly correlate with the cell proliferation inhibitory activity of these compounds. Thus, compounds **7d**, **9f**, and apcin were evaluated by measuring the mitotic cell cycle marker, phosphohistone H3 (PHH3) at serine 10 (**Figure 4A**). **Figure 4B** demonstrated a dose-dependent increase of fluorescence intensity of nuclear phosphohistone H3 levels in the compound-treated cells compared to cells treated with solvent only. The results (**Figure 4C**) showed that **7d** (30 μM) and **9f** (100 μM) induced an increase of phosphohistone H3 positive cells compared to vehicle-treated controls in HepG2 cells for the duration of the treatment (6.9% and 10.0% to 3.8%, respectively). The positive compound, apcin, caused an approximately 2.2-fold increase of PHH3-positive cells compared with the DMSO control. Likewise, a high protein level of phopho-histone H3 in treated cells compared to the control was observed (**Figure 4D**). These results suggested that **7d** and **9f** were more potent than apcin in arresting cells at mitotic exit, and **9f** was the most potent mitotic blocker.

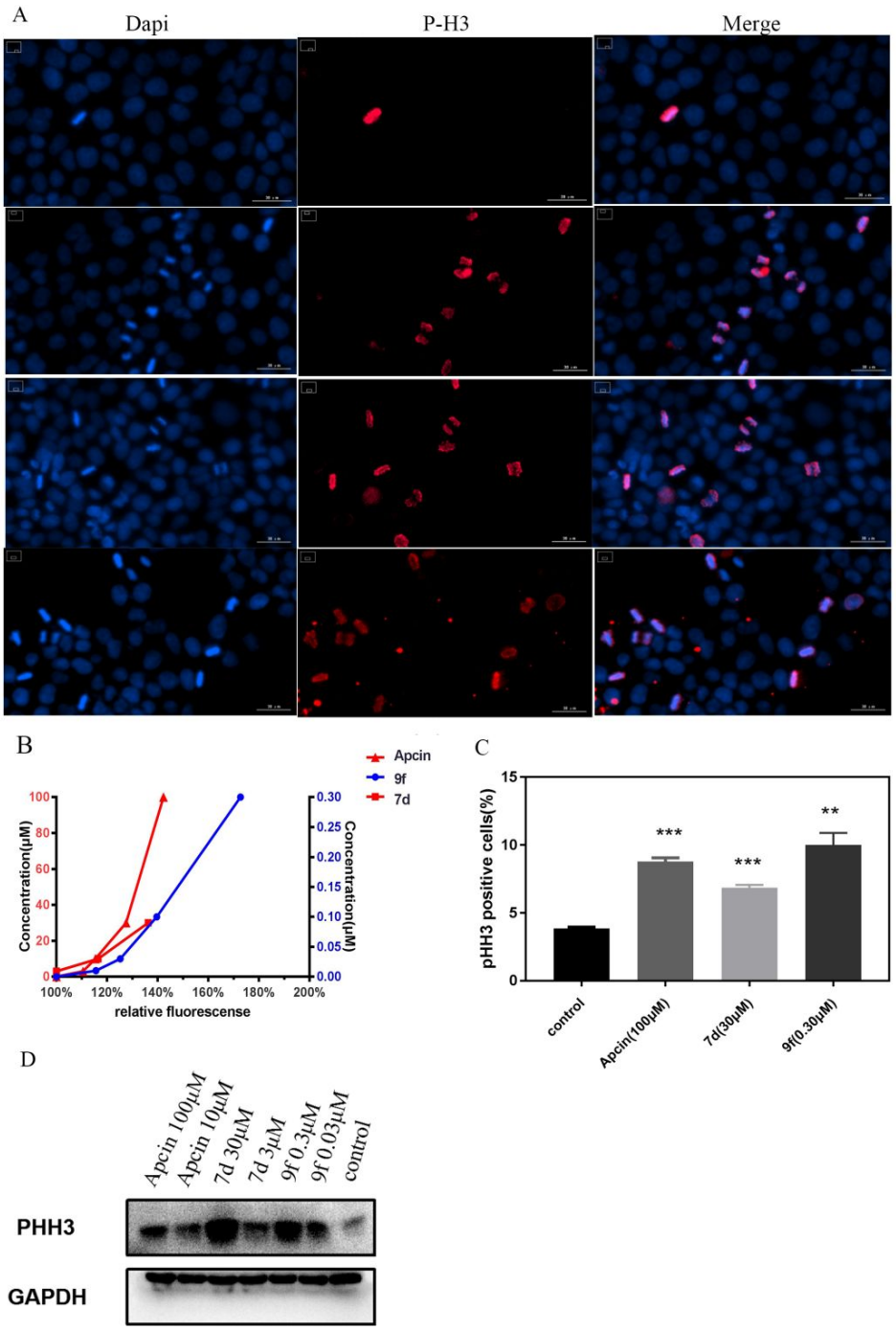

Figure 4. 7d, **9f** blocked mitotic exit. (A) Cells were treated with DMSO (line 1), 100 μM apcin (line 2), 30 μM **7d** (line 3) and 0.3 μM **9f** (line 4) for 48 h, p-Histone H3 (Ser 10) were stained for immunofluorometric analysis, representative images were observed. Cells stained with a specific antibody (red) against phosphohistone H3 (serine 10) and nuclei stained with DAPI (blue) were visualized. (B) Dose-effect curves of **7d** and **9f** were constructed. The relative fluorescence values were measured by comparing to the control group. (C) PHH3-positive cells (red) were counted in randomly selected fields, the histogram showed the mean number of p-histone H3 (Ser 10)-positive cells in the entire population (%). Cells were counted using Image J software. Statistical analysis was performed by SPSS, each treatment group was compared to the control group: (***) $P < 0.001$, (**) $P < 0.01$, (*) $P < 0.05$. (D) PHH3 levels were measured by western blot at 24 h after the addition of compounds. The reproducibility of the results was confirmed by at least two separate experiments.

Compound 9f Disrupted the Organization of the Cellular Microtubule Network As **9f** was much more effective in blocking the cell cycle than in binding to Cdc20, it was suggested that another mechanism of action might exist in **9f**. Since the disruption of microtubule dynamics leads to the formation of aberrant mitotic spindles that are unable to align the chromosomes into the metaphase plate, thereby leading to the accumulation of cells arrested at mitosis, we further examined the inhibitory effects of **9f** on microtubule organization by immunofluorescent staining in HepG2 cells. As shown in **Figure 5**, the microtubule networks in vehicle-treated cells displayed a normal arrangement with fibrous microtubules extending throughout the cell nucleus, providing cellular structure and shape, and bipolar spindle formation was observed. Meanwhile, paclitaxel formed multipolar spindles and bundled microtubules that resulted in aggressive polymerization.[33-34] On the contrary, after exposure to **9f** at 0.3 μM for 48 h, microtubule organization in the cytosol was disrupted and showed condensed chromosomes, indicating that **9f** induced disruption of the microtubule network. These results clearly demonstrate that **9f** exhibited characteristics of tubulin polymerization inhibitors and had a mechanism of action different from that of stabilizing agents such as paclitaxel.

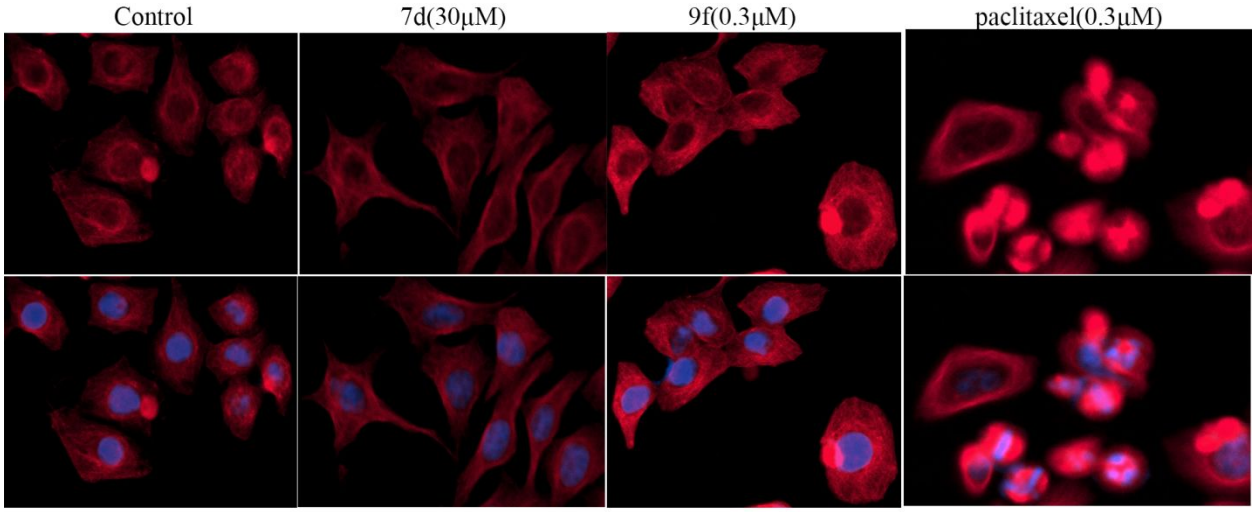

Figure 5. Effects of **7d** and **9f** on the cellular microtubule network were visualized by immunofluorescence. HepG2 cells were treated with vehicle control 0.1% DMSO, 30 μM **7d**, 0.3 μM **9f** and 0.3 μM paclitaxel for 48 h. Then, cells were fixed and stained with anti-α-tubulin antibody (red), and counterstained with DAPI (blue). Detection of the fixed and stained cells was performed using a microplate reader.

To further investigate the effects of **9f** on the assembly kinetics of tubulin in vitro, a tubulin polymerization assay was carried out with the negative control paclitaxel. Accordingly, **9f** inhibited the rate and extent of the assembly of tubulin in a concentration-dependent manner, indicated that **9f** was a potent inhibitor of tubulin assembly (Figure 6). Under similar conditions, paclitaxel promoted the assembly of tubulin as reported.

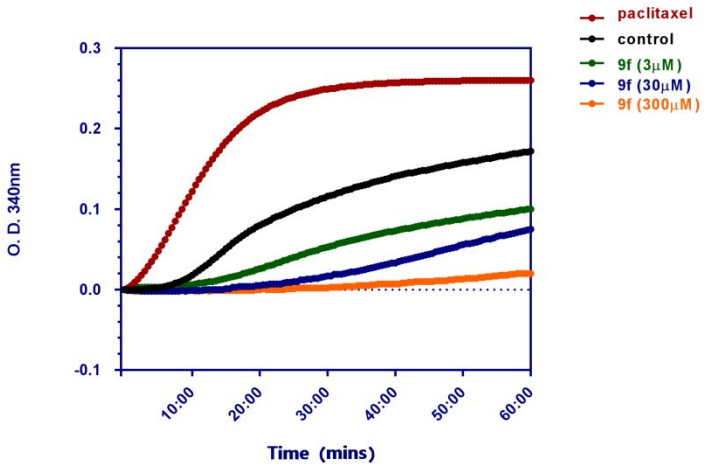

Figure 6. Effect of **9f** on in vitro tubulin polymerization was tested. Polymerization of purified tubulin was performed in a cell-free assay. Tubulin protein was incubated at 37°C in a reaction buffer exposed to vehicle control or test compounds at the indicated concentrations. Absorbance at 340 nm was monitored at 37 °C every 30 s for 60 min.

Results from the analysis of structure−activity relationships for the derivatives indicated that incorporating fluorine at the C-2-position in the adenine ring produced highly potent compounds. To further elucidate how compound **9f** interacted with tubulin, the potential binding mode for **9f** was investigated at three different binding sites occupied by the substituted 5- or 6-membered heterocyclic ring in the tubulin dimer using the molecular operating environment (MOE) 2014 platform.[35-36]

The illustration for the close view of the potential binding pose of **9f** and **01G** (native ligand of tubulin PDB: 2R75) was shown in **Figures 7A and S3**. Generally, **9f** (blue stick) overlapped well with **01G** (green stick) in the same "L" shape. The 2-fluoroadenine ring of **9f** overlapped well with the adenine ring of **01G** and the carbamate overlapped well with the phosphate of **01G**. Similarly, the potential hydrogen bonds were formed between **9f** and Phe179, Asn162, Glu135, Ala67, Thr105, and Gly104. These hydrogen bonds stabilized the interaction of **9f** with the binding pocket. This conclusion was consistent with the X-ray structure of tubulin in complex with the negative ligand, **8Z8** (PDB: 5NJH) and **A9Q** (PDB: 5OSK), respectively.[37] In the binding mode of **Figures 7B and S4**, **9f** (purple stick) was in close proximity to the native ligand **8Z8** (green stick). The adenine occupied the site where the trifluoro-benzene ring in **8Z8** was bound, while the trichloromethyl, which was large steric hindrance of **9f** crossed through the adenine ring in **8Z8**. Two residues, Tyr 210 and Tyr 224, contributed to the strong binding affinity of **8Z8** to tubulin. Moreover, arene-arene interaction between the adenine ring of **9f** and Tyr210, as well as arene-H interaction between the carbon with trichloromethyl substitution of **9f** and Tyr224, were also observed. In addition, the binding mode between **9f** and tubulin was consistent with the observation in 5OSK. Furthermore, key amino acids Cys241 and Lys352 formed an arene-H interaction and hydrogen bond with **A9Q**, respectively. It was noteworthy that because the linker of **9f** projected deeper into the pocket, **9f** had an additional H bond with the surrounding amino acid, Met259 (**Figure 7C and S5**).

In conclusion, compound **9f** inhibited tubulin polymerization in a concentration-dependent manner. The attempts to dock the ligands into the binding site of substituted 5- or 6-membered heterocyclic pointed to the importance of 2-fluoroadenine for the high potency of **9f**.[38]

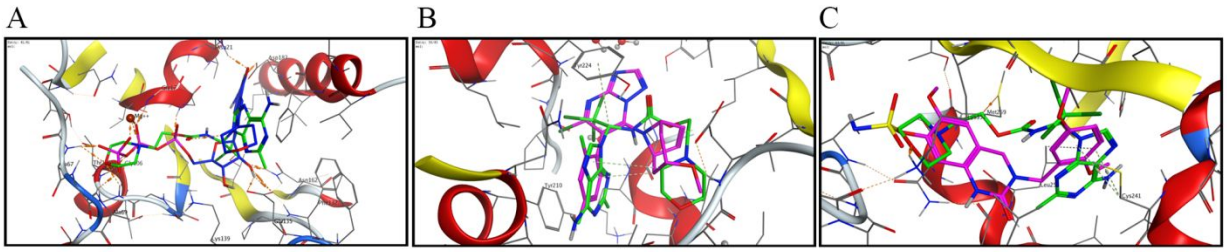

Figure 7. Predicted binding mode of **9f** (green stick) with three different tubulin complex, (A) PDB code: 2R75, (B) PDB code: 5NJH and (C) PDB code: 5OSK, surrounding amino acid residues were labeled. Hydrogen bonds were shown as dotted orange lines.

7d and 9f Induced Cell Apoptosis in HepG2 Cells There is evidence to suggest that execution of cell cycle blockade may induce simultaneous cellular apoptosis. We determined whether **7d** and **9f** could trigger cell apoptosis. The Annexin V-FITC/PI assay was conducted in HepG2 cells which were treated with 100 μM apcin, 30 μM **7d**, and 0.3 μM **9f** for 48 h. A significant increase in the number of apoptotic cells was found after treatment with each compound (**Figure 8A, B**). As shown in **Figure 8C**, **7d** and **9f** induced 34.58 and 42.06% apoptosis at 100 and 0.3 μM, respectively, and apcin caused 14.7% of cells to become apoptotic at 100 μM. In the untreated control, only 9.14% of cells underwent apoptosis. These results indicate that **7d** and **9f** dramatically stimulated cell apoptosis in HepG2 cells, which was consistent with the inhibition of cell proliferation. In order to investigate whether mitotic arrest contributed to the regulation of apoptosis, the levels of the anti-apoptotic BCL-2 family members were examined. The treated cells prompted elevated levels of cleavage of PARP and caspase-3, respectively, with no alternation in the BCL-2 level (**Figure 8D**).

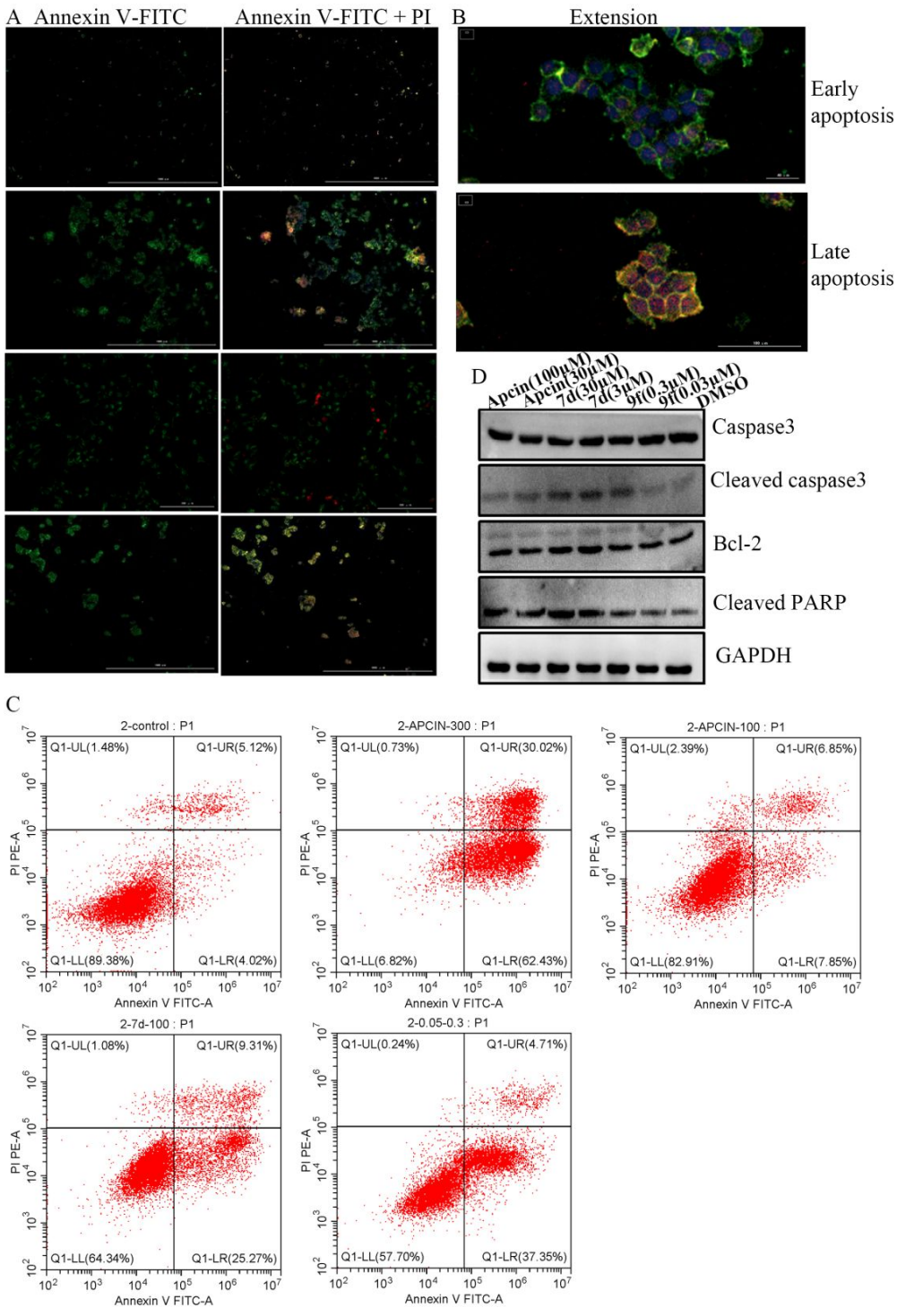

Figure 8. Effects of **7d** and **9f** on apoptosis were tested. (A) Cell apoptosis was conducted in HepG2 cells treated with 100 μM apcin (line 2), 30 μM **7d** (line 3), 0.3 μM **9f** (line 4) and the solvent control (line 1). (B) Representative immunofluorescence images of HepG2 cells showed different phenotypes. The reproducibility of the results was confirmed by at least two separate experiments. (C) Cells were seeded in 6-well plates and treated with compounds for 48 h. Cells were harvested, washed with PBS and resuspended in binding buffer containing PI and FITC-conjugated anti-Annexin V antibody. Apoptosis was analyzed using a flow cytometer. (D) Cells were treated for 48 h. Cell lysate was analyzed to investigate apoptotic cell rate. Endogenous protein levels of caspase3, cleaved caspase3, cleaved PARP and Bcl-2 were determined by Western Blot.

9f Inhibited Cell Migration and Invasion Small molecules with anti-microtubule potency or Cdc20 inhibitory effect have been reported to interfere with tumor cell migration and invasion. To investigate the inhibition of migration by **9f**, a scratch assay was used to detect the migratory activity in HepG2 cells after **9f** treatment. Results from wound healing assays suggested that **9f** remarkably suppressed cell migration in a dose-dependent manner (**Figures 9A, B and S6**). To further explore whether **9f** played a key role in the regulation of hepatoma carcinoma cell motility, an invasion assay was performed in HepG2 cells treated with 0.3 μM **9f** for 48 h. It was demonstrated that compound **9f** significantly retarded the penetration of HepG2 cells through the Matrigel-coated membrane, suggesting that **9f** inhibited cell invasion in HepG2 cells (**Figure 9C, D**). Altogether, **9f** inhibited cell motility in hepatoma carcinoma cells.

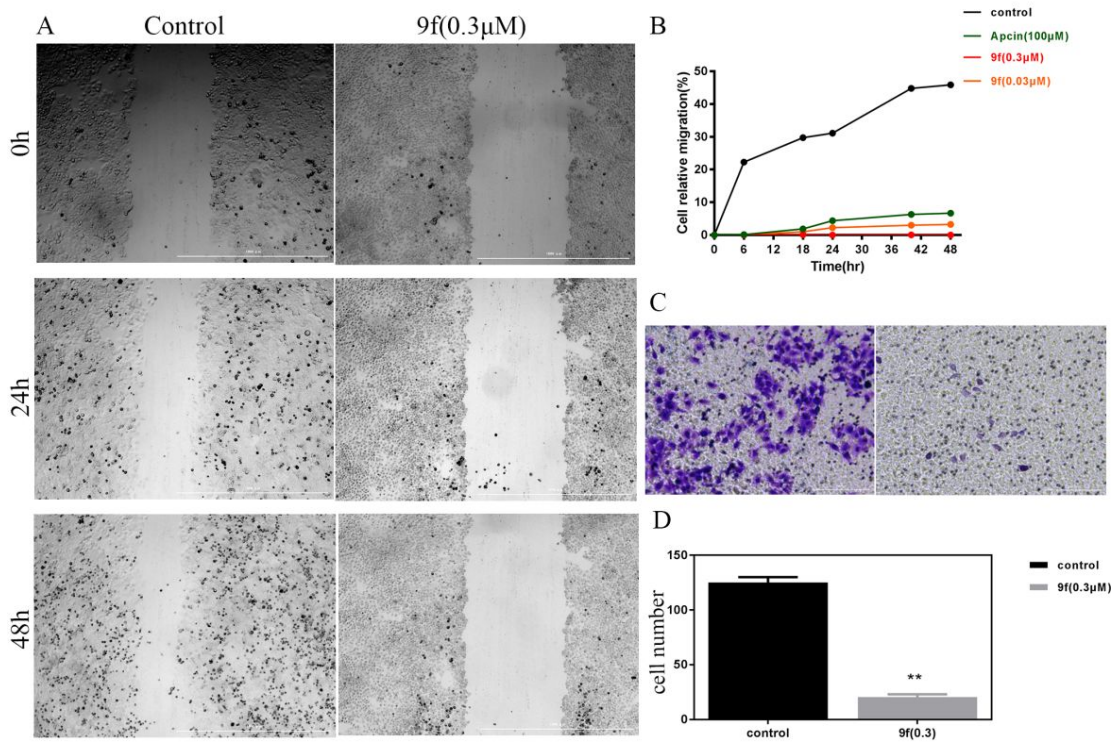

Figure 9. 9f inhibited cell migration and invasion in HepG2 cells. (A) Cell migration was detected using wound healing assay in untreated cells (Left panel) and cells treated with 0.3 μM **9f** (right panel) during 48 h. (B) Quantitative results were illustrated. (C) Left panel: inhibitory effect on invasion in untreated HepG2 cells was determined by Transwell invasion assay, right panel: cells treated with 0.3 μM **9f**. (D) Quantitative results were illustrated.

■ CONCLUSIONS

Cdc20 has been reported to be a critical factor for tumorigenesis, and depleting endogenous Cdc20 in various cancer cell lines leads to a mitotic arrest, followed by aberrant proliferation or apoptotic death.[39] Consistently, evidence from several conditional Cdc20 knockout mouse models suggests that ablation of Cdc20 could completely repress tumors in vivo via apoptosis.[40]

By targeting Cdc20, a series of 2,2,2-trichloro-1-aryl carbamate derivatives (**5a-10c**) were designed, efficiently synthesized, and evaluated in cellular assays. It was reported that low concentrations of apcin did not effectively stabilize the APC/C substrates, which might have been related to the relatively weak interaction between apcin and Cdc20, or the substrates could be recruited to the APC/C through other mechanisms. In this study, **7d** showed higher affinity to Cdc20 than apcin in the SPR study. Correspondingly, treatment of **7d** led to mitotic disturbance and apoptosis, indicating that it might be a promising lead for discovering more potent Cdc20 inhibitors. However, the most potent compound, **9f**, exhibited almost the same binding affinity with Cdc20 as apcin, and further exploration indicated that the nanomolar potency of **9f** against multiple cancer cell lines was due to its additional inhibition of tubulin polymerization. As two critical targets acting at different steps of mitosis, microtubules and Cdc20 are closely linked in function, and the combination of MIAs with APC/C inhibitors seems to be an efficient way to trigger mitotic cells death. Consistently, the implications of paclitaxel/ProTAME combinatorial treatment have been reported to reduce chemoresistance, significantly down-regulate chromosomal instability, and reactivate apoptosis in ovarian cancer and multiple myeloma. Compound **9f** arrested cells in the M phase of the cell cycle, induced HepG2 cell apoptosis, and disrupted cellular microtubules. Mechanistic considerations suggested that the blockade in M

phase of cell cycle was associated with alterations in the expression of cyclins, and the induction of apoptosis was related to activation of caspase-3 and PARP.

In summary, modification of apcin resulted in the discovery of a novel anti-tumor agent as tubulin polymerization and Cdc20 inhibitor. The newly developed compound **9f** showed marked biological activity, and it has the potential for further development as an anti-mitotic agent.

■ EXPERIMENTAL SECTION

General Method Melting points were measured in open capillary tubes on a WRS-2 micro-computer melting point apparatus. All chemical reagents were purchased and used without further purification. All reactions were carried out under an atmosphere of dried nitrogen or argon. Chromatograms were visualized by ultraviolet illumination or by exposure to iodine vapors. Nuclear magnetic resonance (NMR) spectroscopy was carried out on Bruker AVANCEIII-400 and AVANCEIII-500 NMR. Chemical shifts were expressed in parts per million (ppm, δ) downfield from tetramethylsilane (TMS) with coupling constants in hertz (Hz). Multiplicity was described as singlet (s), doublet (d), triplet (t), quartet (q), multiplet (m), and broad (br). High-resolution mass spectra (HRMS) were recorded using an Advion Expression CMS mass spectrometer coupled with an Agilent 1260 analytical HPLC. High-performance liquid chromatography (HPLC) analysis of all final compounds for biological testing were conducted on an Agilent 1260 Series HPLC with an Agilent Extend-C18 column (150×4.6 mm, 5 μm). All final compounds for biological evaluation were analyzed to achieve a minimum of 95% purity. Compound names were derived from the structures using ChemDraw Ultra 14.0.

Chemistry

The readily available substituted ethanol used as the starting material was reacted with 1.2 equivalents of 4-nitrophenyl chloroformate overnight and 1.2 equivalents of anhydrous triethylamine as a base in anhydrous dichloromethane at room temperature. Product carbamate was reacted with 28% aqueous ammonia for 3-24 h. Compounds **4a-f** were synthesized by the treatment of chloral hydrate with carbamate at 80-100℃, adding ethyl acetate, and ultrasonically forming a turbid liquid. The compounds were obtained by suction filtration. The intermediates were ideally poised to undergo chlorination with chlorosulfoxide by refluxing overnight, and then removing residual thionyl chloride until the reaction was completed and subjecting it to a substitution reaction with aromatic amine in the presence of Cs_2CO_3 in acetone. The turbid mixture was filtered and concentrated in vacuo, purification by flash column chromatography on a silica gel to afford the final compounds.

2-(2-methyl-5-nitro-1H-imidazol-1-yl)ethyl(2,2,2-trichloro-1-((4-methylpyrimidin-2-yl) amino)ethyl)carbamate (5b) Following general procedure in Scheme 1 furnished **5b** as white solid. Yield: 21.42%, mp 209.0~209.9℃, HPLC: 97.19%. ^{1}H NMR (500 MHz, DMSO-d_6): δ8.27 (d, J = 5.0 Hz, 1H), 8.00 (s, 1H), 7.97 (d, J = 8.8 Hz, 1H), 6.97 (d, J = 9.5 Hz, 1H), 6.73 (d, J = 5.0 Hz, 1H), 6.60 (t, J = 9.2 Hz, 1H), 4.56-4.46 (m, 3H), 4.35 (dd, J = 10.7, 5.7 Hz, 1H), 2.39 (s, 3H), 2.31 (s, 3H). ^{13}C NMR (126 MHz, DMSO-d_6): δ160.69, 155.24, 152.06, 138.88, 133.53, 112.85, 102.88, 70.12, 63.46, 45.90, 24.10, 14.37. HRMS (ESI) m/z calcd for $[C_{14}H_{16}C_{l3}N_7O_4+H]^+$: 452.0329, found: 452.0401.

(2-methyl-5-nitro-1H-imidazol-1-yl)ethyl(2,2,2-trichloro-1-((4-methoxypyrimidin-2-yl)amino)ethyl)carbamate (5c) Following general procedure in Scheme 1 furnished **5c** as

yellow solid. Yield: 32.66%, mp 81.6~83.3℃, HPLC: 98.63%. ^{1}H NMR (500 MHz, DMSO-d_6): δ8.14 (d, J = 5.7 Hz, 1H), 8.01 (d, J = 16.7 Hz, 2H), 7.05 (s, 1H), 6.57 (d, J = 13.3 Hz, 1H), 6.28 (d, J = 5.7 Hz, 1H), 4.51 (dd, J = 17.4, 4.3 Hz, 3H), 4.38-4.33 (m, 1H), 3.85 (s, 3H), 2.39 (s, 3H). ^{13}C NMR (126 MHz, DMSO-d_6): δ170.22, 160.87, 158.59, 155.27, 152.06, 138.88, 133.51, 102.59, 99.44, 70.35, 63.48, 53.74, 45.89, 14.36. HRMS (ESI) m/z calcd for $[C_{14}H_{16}Cl_3N_7O_5+H]^+$: 468.0278, found: 468.0370.

2-(2-methyl-5-nitro-1H-imidazol-1-yl)ethyl(2,2,2-trichloro-1-((6-oxo-1,6-dihydropyrimidin-2-yl)amino)ethyl)carbamate (5d) Following general procedure in Scheme 1 furnished **5d** as yellow solid. Yield: 16.24%, mp 192.3~193.2℃, HPLC: 98.39%. ^{1}H NMR (500 MHz, DMSO-d_6): δ11.14 (s, 1H), 8.71 (d, J = 8.4 Hz, 1H), 8.01 (s, 1H), 7.64 (d, J = 6.1 Hz, 1H), 7.11 (d, J = 9.3 Hz, 1H), 6.49 (t, J = 9.1 Hz, 1H), 5.72 (d, J = 6.1 Hz, 1H), 4.55-4.48 (m, 3H), 4.37 (dd, J = 7.5, 5.0 Hz, 1H), 2.41 (s, 3H). ^{13}C NMR (126 MHz, DMSO-d_6): δ162.08, 155.74, 155.43, 153.95, 152.10, 138.89, 133.56, 105.94, 101.66, 69.29, 63.28, 46.00, 14.41. HRMS (ESI) m/z calcd for $[C_{13}H_{14}Cl_3N_7O_5+H]^+$: 454.0122, found: 454.0200.

2-(2-methyl-5-nitro-1H-imidazol-1-yl)ethyl(1-((4-aminopyrimidin-2-yl)amino)-2,2,2-trichloroethyl)carbamate (5e) Following general procedure in Scheme 1 furnished **5e** as yellow solid. Yield: 28.69%, mp 104.2~105.0℃, HPLC: 98.55%. ^{1}H NMR (500 MHz, DMSO-d_6): δ8.02 (s, 1H), 7.95 (d, J = 8.5 Hz, 1H), 7.74 (d, J = 5.3 Hz, 1H), 6.64 (s, 2H), 6.53 (t, J = 9.0 Hz, 1H), 6.15 (s, 1H), 5.87 (d, J = 5.1 Hz, 1H), 4.56-4.46 (m, 3H), 4.32 (d, J = 11.4 Hz, 1H), 2.40 (s, 3H). ^{13}C NMR (126 MHz, DMSO-d_6): δ164.54, 160.64, 156.04, 155.13, 152.07, 138.88, 133.52, 103.38, 97.97, 69.98, 63.36, 45.92, 14.37. HRMS (ESI) m/z calcd for $[C_{13}H_{15}Cl_3N_8O_4+H]^+$: 453.0282, found: 453.0360.

(2-methyl-5-nitro-1H-imidazol-1-yl)ethyl(2,2,2-trichloro-1-((4-chloropyrimidin-2-yl)amino) ethyl)carbamate (5f) Following general procedure in Scheme 1 furnished **5f** as white solid. Yield: 20.18%, mp: 182.3~183.4℃, HPLC: 98.75%. ^{1}H NMR (500 MHz, DMSO-d_6): δ8.40 (d, J = 4.8 Hz, 1H), 8.06 (d, J = 8.4 Hz, 1H), 7.99 (s, 1H), 7.87 (s, 1H), 6.98 (d, J = 5.0 Hz, 1H), 6.55 (s, 1H), 4.56–4.47 (m, 3H), 4.40-4.35 (m, 1H), 2.41 (s, 3H). ^{13}C NMR (126 MHz, DMSO-d_6): δ161.18, 155.35, 152.08, 138.90, 133.51, 112.61, 102.13, 70.30, 63.51, 45.88, 14.41. HRMS (ESI) m/z calcd for $[C_{13}H_{13}C_{l4}N_7O_4+H]^+$: 471.9783, found: 471.9864.

(2-methyl-5-nitro-1H-imidazol-1-yl)ethyl(2,2,2-trichloro-1-(pyrimidin-4-ylamino)ethyl) carbamate (6a) Following general procedure in Scheme 1 furnished **6a** as yellow solid. Yield: 32.24%, mp 179.4~180.2℃, HPLC: 99.79%. ^{1}H NMR (500 MHz, DMSO-d_6): δ8.59-8.48 (m, 2H), 8.21 (d, J = 5.9 Hz, 1H), 8.04-7.94 (m, 2H), 6.88 (d, J = 5.9 Hz, 1H), 6.77 (t, J = 8.6 Hz, 1H), 4.50 (d, J = 11.0 Hz, 3H), 4.35 (dd, J =10.7, 4.5 Hz, 1H), 2.39 (s, 3H). ^{13}C NMR (126 MHz, DMSO-d_6): δ161.10, 158.30, 155.81, 155.59, 152.14, 138.87, 133.56, 107.09, 101.98, 68.80, 63.24, 46.04, 14.41. HRMS (ESI) m/z calcd for $[C_{13}H_{14}C_{l3}N_7O_4+H]^+$: 438.0173, found:438.0264.

2-(2-methyl-5-nitro-1H-imidazol-1-yl)ethyl(2,2,2-trichloro-1-(quinolin-2-ylamino)ethyl) carbamate (6b) Following general procedure in Scheme 1 furnished **6b** as yellow solid. Yield: 25.62%, mp 119.9~121.0℃, HPLC: 99.75%. ^{1}H NMR (500 MHz, DMSO-d_6): δ8.35 (d, J = 8.8 Hz, 1H), 8.03–7.98 (m, 2H), 7.71 (d, J = 7.9 Hz, 1H), 7.59-7.54 (m, 2H), 7.49 (d, J = 9.2 Hz, 1H), 7.27 (t, J = 7.2 Hz, 1H), 7.13 (d, J = 8.9 Hz, 1H), 6.94 (t, J = 9.0 Hz, 1H), 4.51 (dd, J = 11.7, 4.8 Hz, 3H), 4.35-4.30 (m, 1H), 2.34 (s, 3H). ^{13}C NMR (126 MHz, DMSO-d_6): δ155.57, 155.16, 152.16, 147.19, 138.82, 137.80, 133.55, 129.84, 127.96, 126.72, 124.23, 123.01, 113.30, 102.69, 69.54, 63.17, 46.07, 14.38. HRMS (ESI) m/z calcd for $[C_{18}H_{17}C_{l3}N_6O_4+H]^+$: 487.0377, found: 487.0463.

2-(2-methyl-5-nitro-1H-imidazol-1-yl)ethyl(2,2,2-trichloro-1-(isoquinolin-3-ylamino)ethyl) carbamate (6c) Following general procedure in Scheme 1 furnished **6c** as yellow solid. Yield: 28.32%, mp 122.6~124.2℃, HPLC: 99.50%. ^{1}H NMR (500 MHz, DMSO-d_6): δ8.96 (s, 1H), 8.27 (d, J = 8.7 Hz, 1H), 7.99 (s, 1H), 7.90 (d, J = 8.2 Hz, 1H), 7.64 (d, J = 8.3 Hz, 1H), 7.58-7.54 (m, 1H), 7.32-7.28 (m, 1H), 7.05 (s, 1H), 6.81-6.72 (m, 2H), 4.49 (d, J = 11.5 Hz, 3H), 4.33 (d, J = 5.3 Hz, 1H), 2.34 (s, 3H). ^{13}C NMR (126 MHz, DMSO-d_6): δ155.57, 152.99, 152.12, 151.48, 138.86, 138.56, 133.53, 131.03, 128.23, 125.27, 124.18, 123.73, 103.23, 100.17, 70.84, 63.23, 46.02, 14.36. HRMS (ESI) m/z calcd for $[C_{18}H_{17}Cl_3N_6O_4+H]^+$: 487.0377, found:487.0469.

2-(2-methyl-5-nitro-1H-imidazol-1-yl)ethyl(2,2,2-trichloro-1-(isoquinolin-1-ylamino)ethyl) carbamate (6d) Following general procedure in Scheme 1 furnished **6d** as white solid. Yield: 27.43%, mp 113.5~114.8℃, HPLC: 97.92%. ^{1}H NMR (500 MHz, DMSO-d_6): δ8.06 (d, J = 8.4 Hz, 1H), 8.02-7.94 (m, 2H), 7.84 (d, J = 8.0 Hz, 1H), 7.78 (d, J = 8.7 Hz, 1H), 7.73 (t, J = 7.5 Hz, 1H), 7.64 (t, J = 7.6 Hz, 1H), 7.35 (d, J = 8.8 Hz, 1H), 7.18 (d, J = 5.7 Hz, 1H), 7.07 (t, J = 8.7 Hz, 1H), 4.49 (dd, J = 21.6, 11.7 Hz, 3H), 4.37-4.31 (m, 1H), 2.36 (s, 3H). ^{13}C NMR (126 MHz, DMSO-d_6): δ155.11, 152.99, 151.98, 140.88, 138.89, 137.32, 133.50, 130.92, 127.44, 127.06, 122.66, 117.67, 113.11, 103.34, 69.26, 63.53, 45.81, 14.34. HRMS (ESI) m/z calcd for $[C_{18}H_{17}Cl_3N_6O_4+H]^+$: 487.0377, found: 487.0463.

2-(2-methyl-5-nitro-1H-imidazol-1-yl)ethyl(1-(1H-benzo[d]imidazol-1-yl)-2,2,2-trichloroethyl)carbamate (6e) Following general procedure in Scheme 1 furnished **6e** as white solid. Yield: 22.13%, mp 123.6~124.9℃, HPLC: 97.97%. ^{1}H NMR (500 MHz, DMSO-d_6): δ 9.68 (d, J = 9.8 Hz, 1H), 8.63 (s, 1H), 8.00 (d, J = 6.1 Hz, 1H), 7.96 (t, J = 11.1 Hz, 1H), 7.71 (t, J = 7.8 Hz, 1H), 7.33 (t, J = 7.4 Hz, 1H), 7.27 (t, J = 7.4 Hz, 1H), 6.88 (t, J = 14.6 Hz, 1H), 4.60-4.51 (m, 3H), 4.40 (dt, J = 8.5, 3.8 Hz, 1H), 2.38 (s, 3H). ^{13}C NMR (126 MHz, DMSO-d_6):

δ155.67, 152.01, 142.82, 142.73, 138.91, 134.14, 133.57, 123.96, 123.03, 120.18, 112.05, 99.86, 73.06, 63.74, 45.86, 14.34. HRMS (ESI) m/z calcd for $[C_{16}H_{15}Cl_3N_6O_4+H]^+$: 461.0220, found: 461.0127.

2-(2-methyl-5-nitro-1H-imidazol-1-yl)ethyl(2,2,2-trichloro-1-((4,6-dichloropyrimidin-2-yl) amino)ethyl)carbamate (7a) Following general procedure in Scheme 1 furnished **7a** as colorless solid. Yield: 46.23%, mp 175.5~176.3℃, HPLC: 99.73%. ^{1}H NMR (500 MHz, DMSO-d_6): δ8.56 (d, J = 9.2 Hz, 1H), 8.17 (d, J = 9.0 Hz, 1H), 7.98 (s, 1H), 7.21 (s, 1H), 6.45 (t, J = 9.1 Hz, 1H), 4.55-4.48 (m, 3H), 4.38 (dt, J = 9.5, 4.4 Hz, 1H), 2.42 (s, 3H). ^{13}C NMR (126 MHz, DMSO-d_6): δ160.73, 155.42, 152.12, 138.90, 133.50, 111.40, 101.52, 70.47, 63.53, 45.90, 14.45. HRMS (ESI) m/z calcd for $[C_{13}H_{12}Cl_5N_7O_4+H]^+$: 505.9393, found: 505.9472.

2-(2-methyl-5-nitro-1H-imidazol-1-yl)ethyl(2,2,2-trichloro-1-((4,6-dichloro-5-methylpyrimidin-2-yl)amino)ethyl)carbamate (7b) Following general procedure in Scheme 1 furnished **7b** as white solid. Yield: 46.66%, mp 140.3~142.1℃, HPLC: 99.82%. ^{1}H NMR (400 MHz, DMSO-d_6): δ8.24 (d, J = 9.3 Hz, 1H), 8.15 (d, J = 9.0 Hz, 1H), 7.99 (s, 1H), 6.40 (t, J = 9.1 Hz, 1H), 4.56-4.46 (m, 3H), 4.37 (dt, J = 9.3, 3.9 Hz, 1H), 2.42 (s, 3H), 2.26 (s, 3H). ^{13}C NMR (101 MHz, DMSO-d_6): δ158.23, 155.43, 152.15, 138.90, 133.55, 117.65, 101.74, 70.55, 63.51, 45.92, 15.41, 14.47. HRMS (ESI) m/z calcd for $[C_{14}H_{14}Cl_5N_7O_4+H]^+$: 519.9550, found: 519.9629.

2-(2-methyl-5-nitro-1H-imidazol-1-yl)ethyl(1-((5-amino-4,6-dichloropyrimidin-2-yl)amino)-2,2,2-trichloroethyl)carbamate (7c) Following general procedure in Scheme 1 furnished **7c** as yellow solid. Yield: 27.68%, mp 92.9~93.7℃, HPLC: 99.73%. ^{1}H NMR (500 MHz, DMSO-d_6): δ8.00 (d, J = 8.9 Hz, 1H), 7.98 (s, 1H), 7.21 (d, J = 9.5 Hz, 1H), 6.26 (t, J = 9.2 Hz, 1H), 5.16 (s,

2H), 4.56-4.45 (m, 3H), 4.37 (dt, *J* = 9.6, 4.6 Hz, 1H), 2.40 (s, 3H). ^{13}C NMR (126 MHz, DMSO-d_6): δ155.34, 152.07, 151.11, 145.55, 138.88, 133.49, 129.80, 102.40, 71.00, 63.41, 45.92, 14.40. HRMS (ESI) m/z calcd for $[C_{13}H_{13}Cl_5N_8O_4+H]^+$: 520.9502, found: 520.9581.

2-(2-methyl-5-nitro-1H-imidazol-1-yl)ethyl(1-((2-amino-4,6-dichloropyrimidin-5-yl)amino)-2,2,2-trichloroethyl) carbamate (7d) Following general procedure in Scheme 1 furnished **7d** as white solid. Yield: 20.18%, mp 125.1~125.7℃, HPLC: 99.14%. ^{1}H NMR (500 MHz, DMSO-d_6): δ8.35 (s, 1H), 8.34 (d, *J* = 9.5 Hz, 1H), 8.01 (s, 1H), 7.76-7.74 (m, 1H), 7.26 (s, 2H), 5.58 (t, *J* = 10.0 Hz, 1H), 4.61 (d, *J* = 10.6 Hz, 1H), 4.47 (d, *J* = 11.9 Hz, 3H), 4.42–4.35 (m, 1H), 2.40 (s, 3H). ^{13}C NMR (126 MHz, DMSO-d_6): δ158.85, 156.40, 155.83, 152.17, 138.83, 133.53, 121.90, 102.23, 75.27, 63.21, 46.09, 14.45. HRMS (ESI) m/z calcd for $[C_{13}H_{13}Cl_5N_8O_4+H]^+$: 520.9502, found: 520.9574.

2-(2-methyl-5-nitro-1H-imidazol-1-yl)ethyl(2,2,2-trichloro-1-(6-chloro-9H-purin-9-yl)ethyl) carbamate (8a) Following general procedure in Scheme 1 furnished **8a** as colorless solid. Yield: 21.32%, mp 101.4~101.8℃, HPLC: 96.82%. ^{1}H NMR (500 MHz, DMSO-d_6): δ9.76 (d, *J* = 10.0 Hz, 1H), 8.98 (s, 1H), 8.93 (s, 1H), 7.91 (s, 1H), 7.00 (d, *J* = 10.0 Hz, 1H), 4.57-4.45 (m, 4H), 2.37 (s, 3H). ^{13}C NMR (126 MHz, DMSO-d_6): δ155.56, 153.11, 152.38, 151.86, 150.38, 144.65, 138.98, 133.45, 130.31, 98.77, 71.56, 63.87, 45.75, 14.35. HRMS (ESI) m/z calcd for $[C_{14}H_{12}Cl_4N_8O_4+H]^+$: 496.9736, found: 496.9782.

2-(2-methyl-5-nitro-1H-imidazol-1-yl)ethyl(2,2,2-trichloro-1-(6-(dimethylamino)-9H-purin-9-yl)ethyl)carbamate (8b) Following general procedure in Scheme 1 furnished **8b** as white solid. Yield: 20.23%, mp 113.6~115.2℃, HPLC: 98.22%. ^{1}H NMR (500 MHz, $CDCl_3$): δ8.51 (s, 1H), 8.31 (s, 1H), 7.96 (s, 1H), 7.94 (s, 1H), 6.65 (d, *J* = 9.7 Hz, 1H), 4.64-4.58 (m, 3H), 4.54-4.49 (m,

1H), 3.58 (s, 6H), 2.47 (s, 3H). ^{13}C NMR (126 MHz, DMSO-d_6): δ155.52, 154.74, 153.01, 151.93, 151.01, 138.94, 137.06, 133.50, 118.26, 99.65, 70.73, 63.80, 45.81, 14.32. HRMS (ESI) m/z calcd for $[C_{16}H_{18}Cl_3N_9O_4+H]^+$: 506.0547, found: 506.0638.

2-(2-methyl-5-nitro-1H-imidazol-1-yl)ethyl(1-(6-benzamido-9H-purin-9-yl)-2,2,2-trichloroethyl)carbamate (8c) Following general procedure in Scheme 1 furnished **8**c as white solid. Yield: 22.65%, mp 183.7~184.9℃, HPLC: 97.27%. ^{1}H NMR (500 MHz, DMSO-d_6): δ11.35 (s, 1H), 9.71 (d, J = 9.9 Hz, 1H), 8.85 (s, 1H), 8.78 (s, 1H), 8.06 (d, J = 7.4 Hz, 2H), 7.97 (s, 1H), 7.66 (t, J = 7.2 Hz, 1H), 7.57 (t, J = 7.3 Hz, 2H), 7.05 (d, J = 9.9 Hz, 1H), 4.58 (d, J = 11.0 Hz, 3H), 4.45 (s, 1H), 2.38 (s, 3H). ^{13}C NMR (126 MHz, DMSO-d_6): δ166.08, 155.59, 152.94, 152.91, 151.92, 151.30, 141.70, 138.97, 133.61, 133.49, 133.05, 129.01, 128.97, 124.43, 99.26, 71.09, 63.89, 45.78, 14.33. HRMS (ESI) m/z calcd for $[C_{21}H_{18}Cl_3N_9O_5+H]^+$: 582.0496, found: 582.0577.

2-(2-methyl-5-nitro-1H-imidazol-1-yl)ethyl(1-(6-(benzylamino)-9H-purin-9-yl)-2,2,2-trichloroethyl)carbamate (8d) Following general procedure in Scheme 1 furnished **8d** as white solid. Yield: 23.21%, mp 121.0~121.8℃, HPLC: 98.42%. ^{1}H NMR (500 MHz, DMSO-d_6): δ 9.60 (d, J = 10.1 Hz, 1H), 8.60 (s, 1H), 8.48 (s, 1H), 8.29 (s, 1H), 7.98 (s, 1H), 7.35 (d, J = 7.4 Hz, 2H), 7.29 (t, J = 7.5 Hz, 2H), 7.21 (t, J = 7.2 Hz, 1H), 6.92 (d, J = 10.1 Hz, 1H), 4.72 (s, 2H), 4.56 (t, J = 9.3 Hz, 3H), 4.42 (dd, J = 8.8, 5.6 Hz, 1H), 2.38 (s, 3H). ^{13}C NMR (126 MHz, DMSO-d_6): δ155.52, 154.90, 153.76, 151.93, 149.63, 140.31, 138.94, 138.30, 133.50, 128.68, 127.68, 127.13, 118.14, 99.55, 70.82, 63.81, 45.80, 43.45, 14.33. HRMS (ESI) m/z calcd for $[C_{21}H_{20}Cl_3N_9O_4+H]^+$: 568.0704, found: 568.0795.

2-(2-methyl-5-nitro-1H-imidazol-1-yl)ethyl(1-(6-amino-2-chloro-9H-purin-9-yl)-2,2,2-trichloroethyl)carbamate (8e) Following general procedure in Scheme 1 furnished **8e** as white solid. Yield: 20.18%, mp 196.5~197.6℃, HPLC: 98.62%. ^{1}H NMR (500 MHz, DMSO-d_6): δ9.61 (d, J = 10.0 Hz, 1H), 8.45 (s, 1H), 7.99 (d, J = 20.3 Hz, 3H), 6.73 (d, J = 9.8 Hz, 1H), 4.57 (d, J = 9.3 Hz, 3H), 4.44 (d, J = 8.1 Hz, 1H), 2.38 (s, 3H). ^{13}C NMR (126 MHz, DMSO-d_6): δ157.40, 155.54, 154.23, 151.91, 151.23, 138.96, 138.72, 133.47, 116.94, 99.23, 70.90, 63.85, 45.79, 14.32. HRMS (ESI) m/z calcd for $[C_{14}H_{13}Cl_4N_9O_4+H]^+$: 511.9845, found: 511.9915.

2-(2-methyl-5-nitro-1H-imidazol-1-yl)ethyl(2,2,2-trichloro-1-(2,6-diamino-9H-purin-9-yl)ethyl)carbamate (8f) Following general procedure in Scheme 1 furnished **8f** as yellow solid. Yield: 25.3 %, mp 165.8~166.6℃, HPLC: 98.68%. ^{1}H NMR (400 MHz, DMSO-d_6): δ9.47 (d, J = 10.2 Hz, 1H), 8.03 (d, J = 7.8 Hz, 2H), 6.85 (s, 2H), 6.73 (d, J = 10.1 Hz, 1H), 6.07 (s, 2H), 4.58 (ddd, J = 16.2, 9.9, 5.1 Hz, 3H), 4.39 (dd, J = 7.6, 4.6 Hz, 1H), 2.40 (s, 3H). ^{13}C NMR (101 MHz, DMSO-d_6): δ161.21, 156.74, 155.56, 152.60, 152.00, 138.97, 134.48, 133.53, 111.95, 100.10, 70.22, 63.64, 45.88, 14.35. HRMS (ESI) m/z calcd for $[C_{14}H_{15}Cl_3N_{10}O_4+H]^+$: 493.0343, found: 493.0416.

2-(2-methyl-5-nitro-1H-imidazol-1-yl)ethyl(1-(6-amino-2-fluoro-9H-purin-9-yl)-2,2,2-trichloroethyl)carbamate (8g) Following general procedure in Scheme 1 furnished **8g** as white solid. Yield: 19.26%, mp 168.1~169.6℃, HPLC: 96.92%. ^{1}H NMR (500 MHz, DMSO-d_6): δ9.60 (d, J = 10.0 Hz, 1H), 8.42 (s, 1H), 8.00 (d, J = 31.1 Hz, 3H), 6.70 (d, J = 10.0 Hz, 1H), 4.57 (d, J = 10.1 Hz, 3H), 4.44 (d, J = 7.5 Hz, 1H), 2.38 (s, 3H). ^{13}C NMR (126 MHz, DMSO-d_6): δ160.25, 158.62, 158.40, 158.23, 155.54, 151.91, 151.71, 151.55, 138.96, 138.61, 133.46, 116.28, 99.26, 71.02, 63.85, 45.79, 14.30. HRMS (ESI) m/z calcd for $[C_{14}H_{13}Cl_3FN_9O_4+H]^+$: 496.0140, found: 496.0222.

2-(2-methyl-5-nitro-1H-imidazol-1-yl)ethyl(1-(2-amino-6-chloro-9H-purin-9-yl)-2,2,2-trichloroethyl)carbamate (8h) Following general procedure in Scheme 1 furnished **8h** as white solid. Yield: 22.16%, mp 140.4~140.9℃, HPLC: 97.69%. ^{1}H NMR (500 MHz, DMSO-d_6): δ9.61 (d, J = 9.9 Hz, 1H), 8.40 (s, 1H), 7.96 (s, 1H), 7.26 (s, 2H), 6.78 (d, J = 10.0 Hz, 1H), 4.53 (t, J = 35.8 Hz, 4H), 2.38 (s, 3H). ^{13}C NMR (126 MHz, DMSO-d_6): δ160.75, 155.58, 154.62, 151.90, 150.53, 139.79, 139.01, 133.45, 122.32, 99.33, 70.70, 63.74, 45.83, 14.33. HRMS (ESI) m/z calcd for $[C_{14}H_{13}Cl_4N_9O_4+H]^+$: 511.9845, found: 511.9923.

2-(2-methyl-5-nitro-1H-imidazol-1-yl)ethyl(2,2,2-trichloro-1-(6-chloro-2-fluoro-9H-purin-9-yl)ethyl)carbamate (8i) Following general procedure in Scheme 1 furnished **8i** as white solid. Yield: 23.16%, mp 171.3~172.9℃, HPLC: 98.85%. ^{1}H NMR (500 MHz, DMSO-d_6): δ9.80 (d, J = 9.7 Hz, 1H), 8.97 (s, 1H), 7.92 (s, 1H), 6.82 (d, J = 10.0 Hz, 1H), 4.60-4.47 (m, 4H), 2.38 (s, 3H). ^{13}C NMR (126 MHz, DMSO-d_6): δ157.93, 156.21, 155.56, 154.42, 154.28, 152.12, 151.98, 151.87, 145.47, 138.99, 133.39, 129.60, 98.42, 71.92, 63.92, 45.76, 14.36. HRMS (ESI) m/z calcd for $[C_{14}H_{11}Cl_4N_8O_4+H]^+$: 514.9641, found: 514.9718.

2-(2-methyl-5-nitro-1H-imidazol-1-yl)ethyl(1-(2-amino-6-(benzyloxy)-9H-purin-9-yl)-2,2,2-trichloroethyl)carbamate (8j) Following general procedure in Scheme 1 furnished **8j** as white solid. Yield: 24.53%, mp 171.6~172.8℃, HPLC: 96.77%. ^{1}H NMR (500 MHz, DMSO-d_6): δ9.54 (d, J = 10.1 Hz, 1H), 8.17 (s, 1H), 8.00 (s, 1H), 7.52 (d, J = 7.3 Hz, 2H), 7.40 (t, J = 7.3 Hz, 2H), 7.38-7.34 (m, 1H), 6.79 (d, J = 7.3 Hz, 3H), 5.50 (s, 2H), 4.56 (t, J = 10.3 Hz, 3H), 4.41 (d, J = 10.3 Hz, 1H), 2.39 (s, 3H). ^{13}C NMR (126 MHz, DMSO-d_6): δ160.69, 155.57, 155.03, 151.95, 138.98, 136.91, 136.74, 133.50, 129.04, 128.89, 128.59, 112.66, 99.77, 70.47, 67.61, 63.68, 45.86, 14.33. HRMS (ESI) m/z calcd for $[C_{21}H_{20}Cl_3N_9O_5+H]^+$: 584.0653, found:584.0735.

2-(2-methyl-5-nitro-1H-imidazol-1-yl)ethyl(2,2,2-trichloro-1-(2,6-dichloro-9H-purin-9-yl)ethyl)carbamate (8k) Following general procedure in Scheme 1 furnished **8k** as white solid. Yield: 19.33%, mp 129.9~131.7℃, HPLC: 99.76%. ^{1}H NMR (500 MHz, DMSO-d_6): δ9.77 (d, J = 9.8 Hz, 1H), 9.01 (d, J = 21.3 Hz, 1H), 7.91 (s, 1H), 6.86 (d, J = 9.8 Hz, 1H), 4.59-4.46 (m, 4H), 2.37 (s, 3H). ^{13}C NMR (126 MHz, DMSO-d_6): δ155.56, 153.83, 152.55, 151.87, 151.22, 145.42, 139.01, 133.38, 130.10, 98.46, 71.80, 63.92, 45.76, 14.37. HRMS (ESI) m/z calcd for $[C_{14}H_{11}Cl_5N_8O_4+H]^+$: 530.9346, found: 530.9421.

2-(2-methyl-5-nitro-1H-imidazol-1-yl)ethyl(1-(2-acetamido-6-oxo-3,6-dihydro-9H-purin-9-yl)-2, 2, 2-trichloroethyl)carbamate (8l) Following general procedure in Scheme 1 furnished **8l** as colorless solid. Yield: 22.16%, mp 197.5~198.3℃, HPLC: 99.67%. ^{1}H NMR (500 MHz, DMSO-d_6): δ12.13 (s, 1H), 11.90 (s, 1H), 9.67 (d, J = 9.1 Hz, 1H), 8.29 (s, 1H), 7.99 (s, 1H), 6.76 (d, J = 9.8 Hz, 1H), 4.50 (d, J = 54.2 Hz, 4H), 2.38 (s, 3H), 2.19 (s, 3H). ^{13}C NMR (126 MHz, DMSO-d_6): δ174.19, 155.64, 155.20, 151.91, 149.53, 149.04, 139.04, 136.98, 133.50, 119.25, 99.23, 70.80, 63.69, 45.89, 24.24, 14.32.HRMS (ESI) m/z calcd for $[C_{16}H_{16}Cl_3N_9O_6+H]^+$: 536.0289, found: 536.0362.

2-(2-methyl-5-nitro-1H-imidazol-1-yl)ethyl(1-(6-amino-9H-purin-9-yl)-2,2,2-trichloroethyl) carbamate (8m) Following general procedure in Scheme 1 furnished **8m** as white solid. Yield: 12.36%, mp 187.1~187.9℃, HPLC: 98.68%. ^{1}H NMR (400 MHz, DMSO-d_6): δ9.59 (d, J = 10.1 Hz, 1H), 8.46 (s, 1H), 8.21 (s, 1H), 7.98 (s, 1H), 7.48 (s, 2H), 6.89 (d, J = 10.1 Hz, 1H), 4.61-4.52 (m, 3H), 4.47-4.39 (m, 1H), 2.38 (s, 3H). ^{13}C NMR (101 MHz, DMSO-d_6): δ156.60, 155.57, 153.74, 151.98, 150.22, 138.96, 138.31, 133.47, 117.59, 99.66, 70.90, 63.84, 45.90, 14.51. HRMS (ESI) m/z calcd for $[C_{14}H_{14}Cl_3N_9O_4+H]^+$: 478.0234, found: 478.0313.

Benzyl (1-(6-amino-2-chloro-9H-purin-9-yl)-2,2,2-trichloroethyl)carbamate (9a) Following general procedure in Scheme 1 furnished **9a** as white solid. Yield: 21.32%, mp 198.6~199.9℃, HPLC: 98.49%. ^{1}H NMR (400 MHz, DMSO-d_6): δ9.69 (d, J = 10.1 Hz, 1H), 8.49 (s, 1H), 8.05 (s, 2H), 7.37 (dd, J = 15.1, 7.4 Hz, 5H), 6.87 (d, J = 10.2 Hz, 1H), 5.21–5.12 (m, 2H). ^{13}C NMR (101 MHz, DMSO-d_6): δ157.42, 155.85, 154.31, 151.25, 138.78, 136.18, 128.95, 128.86, 128.80, 116.92, 99.48, 70.91, 67.70. HRMS (ESI) m/z calcd for $[C_{15}H_{12}Cl_4N_6O_2+H]^+$: 448.9776, found: 448.9853.

(1-methyl-5-nitro-1H-imidazol-2-yl)methyl(1-(6-amino-2-chloro-9H-purin-9-yl)-2,2,2-trichloroethyl)carbamate (9b) Following general procedure in Scheme 1 furnished **9b** as white solid. Yield: 23.16%, mp 185.8~186.3℃, HPLC: 98.24%. ^{1}H NMR (500 MHz, DMSO-d_6): δ9.87 (d, J = 10.0 Hz, 1H), 8.48 (s, 1H), 8.06 (d, J = 12.8 Hz, 3H), 6.83 (d, J = 10.0 Hz, 1H), 5.32 (q, J = 13.6 Hz, 2H), 3.91 (s, 3H). ^{13}C NMR (126 MHz, DMSO-d_6): δ157.42, 155.27, 154.30, 151.26, 147.57, 139.93, 138.75, 132.24, 116.90, 99.37, 70.93, 59.34, 33.98. HRMS (ESI) m/z calcd for $[C_{13}H_{11}Cl_4N_9O_4+H]^+$: 497.9688, found: 497.9766.

Ethyl(1-(6-amino-2-chloro-9H-purin-9-yl)-2,2,2-trichloroethyl)carbamate (9c) Following general procedure in Scheme 1 furnished **9c** as white solid. Yield: 19.89%, mp 219.5~220.4℃, HPLC: 98.67%. ^{1}H NMR (400 MHz, DMSO-d_6): δ9.53 (d, J = 10.2 Hz, 1H), 8.51 (s, 1H), 8.04 (s, 2H), 6.83 (d, J = 10.2 Hz, 1H), 4.14 (ddd, J = 10.7, 7.0, 3.7 Hz, 2H), 1.22 (t, J = 7.1 Hz, 3H). ^{13}C NMR (101 MHz, DMSO-d_6): δ157.42, 155.92, 154.28, 151.25, 138.86, 116.91, 99.57, 70.85, 62.25, 14.77. HRMS (ESI) m/z calcd for $[C_{10}H_{10}Cl_4N_6O_2+H]^+$: 386.9616, found: 386.96970.

(1-methyl-5-nitro-1H-imidazol-2-yl)methyl(1-(6-amino-2-fluoro-9H-purin-9-yl)-2,2,2-trichloroethyl)carbamate (9d) Following general procedure in Scheme 1 furnished **9d** as white

solid. Yield: 21.63%, mp 205.8~206.9℃, HPLC: 99.00%. ^{1}H NMR (500 MHz, DMSO-d_6): δ9.85 (d, J = 9.9 Hz, 1H), 8.45 (s, 1H), 8.04 (d, J = 24.3 Hz, 3H), 6.80 (d, J = 9.9 Hz, 1H), 5.33 (q, J = 13.6 Hz, 2H), 3.92 (s, 3H). ^{13}C NMR (126 MHz, DMSO-d_6): δ160.29, 158.66, 158.41, 158.24, 155.26, 151.73, 151.57, 147.58, 139.91, 138.62, 132.22, 116.24, 102.69, 99.37, 84.10, 71.03, 59.33, 33.96. HRMS (ESI) m/z calcd for $[C_{13}H_{11}Cl_4N_9O_4+H]^+$: 481.9984, found:482.0055.

Ethyl(1-(6-amino-2-fluoro-9H-purin-9-yl)-2,2,2-trichloroethyl)carbamate (9e) Following general procedure in Scheme 1 furnished **9e** as white solid. Yield: 18.21%, mp 208.3~209.8℃, HPLC: 99.12%. ^{1}H NMR (400 MHz, DMSO-d_6): δ9.50 (d, J = 10.1 Hz, 1H), 8.48 (s, 1H), 8.05 (d, J = 45.7 Hz, 2H), 6.80 (d, J = 10.2 Hz, 1H), 4.14 (dd, J = 13.3, 6.4 Hz, 2H), 1.21 (t, J = 7.0 Hz, 3H). ^{13}C NMR (101 MHz, DMSO-d_6): δ160.29, 158.65, 158.41, 158.24, 155.91, 151.73, 151.57, 138.73, 116.29, 116.26, 99.60, 70.96, 62.21, 14.75. HRMS (ESI) m/z calcd for $[C_{10}H_{10}Cl_4N_6O_2+H]^+$: 370.9915, found: 370.9988.

2-morpholinoethyl(1-(6-amino-2-fluoro-9H-purin-9-yl)-2,2,2-trichloroethyl)carbamate (9f) Following general procedure in Scheme 1 furnished **9f** as colorless solid. Yield: 10.42%, mp 160.2~161.4℃, HPLC: 96.96%. ^{1}H NMR (500 MHz, DMSO-d_6): δ9.68 (d, J = 9.1 Hz, 1H), 8.55 (s, 1H), 8.03 (d, J = 38.0 Hz, 2H), 6.79 (d, J = 10.0 Hz, 1H), 4.21 (s, 2H), 3.03 (d, J = 7.3 Hz, 4H), 2.60 (s, 2H), 2.46 (s, 4H). ^{13}C NMR (126 MHz, DMSO-d_6): δ158.32, 155.78, 138.96, 130.10, 102.96, 99.51, 83.94, 71.03, 70.20, 65.69, 56.68, 53.32. HRMS (ESI) m/z calcd for $[C_{14}H_{18}Cl_3FN_7O_3+H]^+$: 456.0515, found: 456.0517.

2-morpholinoethyl(2,2,2-trichloro-1-(2,6-diamino-9H-purin-9-yl)ethyl)carbamate (9g) Following general procedure in Scheme 1 furnished **9g** as white solid. Yield: 10.07%, mp 145.4~145.8℃, HPLC: 97.8%. ^{1}H NMR (500 MHz, DMSO-d_6): δ9.44 (d, J = 10.1 Hz, 1H), 8.11

(s, 1H), 6.90–6.80 (m, 3H), 6.08 (s, 2H), 4.18 (s, 2H), 3.51 (s, 4H), 2.51 (s, 2H), 2.38 (s, 4H). NMR HRMS (ESI) m/z calcd for $[C_{14}H_{19}Cl_3N_8O_3+H]^+$: 453.0718, found: 453.0724.

2-(pyridin-2-yl)ethyl(1-(6-amino-2-fluoro-9H-purin-9-yl)-2,2,2-trichloroethyl)carbamate (9h) Following general procedure in Scheme 1 furnished **9h** as white solid. Yield: 26.58%, mp 100.9~102.5℃, HPLC: 97.28%. ^{1}H NMR (500 MHz, DMSO-d_6): δ9.78 (d, J = 9.7 Hz, 1H), 8.75 (s, 1H), 8.55 (s, 1H), 8.37 (s, 1H), 8.07-7.92 (m, 3H), 7.81 (s, 1H), 6.70 (d, J = 9.9 Hz, 1H), 4.51 (d, J = 6.9 Hz, 2H), 3.39 (s, 2H). ^{13}C NMR (126 MHz, DMSO-d_6): δ160.22 (s), 158.58 (s), 158.33 (s), 158.16, 155.69 (s), 154.21 (s), 142.99 (s), 139.02 (d), 127.59 (s), 125.26 (s), 116.20 (s), 99.37 (s), 70.98 (s), 64.02 (s), 33.43 (s). HRMS (ESI) m/z calcd for $[C_{15}H_{13}Cl_3FN_7O_2+H]^+$: 448.0253, **found:** 448.0257

2-(pyridin-2-yl)ethyl(2,2,2-trichloro-1-(2,6-diamino-9H-purin-9-yl)ethyl)carbamate (9i) Following general procedure in Scheme 1 furnished **9i** as white solid. Yield: 27.38 %, mp 119.6-122.0℃, HPLC: 95.32%. ^{1}H NMR (500 MHz, DMSO-d_6): δ9.34 (d, J = 10.1 Hz, 1H), 8.48 (d, J = 3.9 Hz, 1H), 8.07 (s, 1H), 7.69 (t, J = 7.1 Hz, 1H), 7.29 (d, J = 7.6 Hz, 1H), 7.24-7.19 (m, 1H), 6.91-6.77 (m, 3H), 6.08 (s, 2H), 4.52-4.43 (m, 2H), 3.08 (t, J = 6.5 Hz, 2H). ^{13}C NMR (126 MHz, DMSO-d_6): δ161.23 (s), 158.02 (s), 156.75 (s), 152.59 (s), 149.56 (s), 137.00 (s), 134.68 (s), 123.90 (s), 122.23 (s), 111.95 (s), 100.45 (s), 70.19 (s), 64.90 (s), 60.23 (s), 37.14 (s).HRMS (ESI) m/z calcd for $[C_{15}H_{15}Cl_3N_8O_2+H]^+$: 445.0456, found: 445.0460.

2-morpholinoethyl(1-(4-amino-1H-pyrazolo[3,4-d]pyrimidin-1-yl)-2,2,2-trichloroethyl) carbamate (10a) Following general procedure in Scheme 1 furnished **10a** as white solid. Yield: 19.56%, mp 164.0~165.2℃, HPLC: 96.8%. ^{1}H NMR (500 MHz, DMSO-d_6): δ9.27 (d, J = 7.9 Hz, 1H), 8.38 (s, 1H), 8.22 (d, J = 23.0 Hz, 2H), 7.79 (s, 1H), 7.15 (d, J = 9.7 Hz, 1H), 4.14 (s,

2H), 3.48 (s, 4H), 2.51 (s, 2H), 2.37 (s, 4H). ^{13}C NMR (126 MHz, DMSO-d_6): δ158.49, 157.03, 156.26, 155.34, 135.09, 99.91, 99.65, 71.72, 66.48, 62.90, 57.14, 53.79. HRMS (ESI) m/z calcd for $[C_{14}H_{18}Cl_3N_7O_3+H]^+$: 438.0604, found: 438.0610.

2-(pyridin-2-yl)ethyl(2,2,2-trichloro-1-(4-((2,2,2-trichloro-1-(((2-(pyridin-2-yl)ethoxy) carbonyl)amino)ethyl)amino)-1H-pyrazolo[3,4-d]pyrimidin-1-yl)ethyl)carbamate (10b) Following general procedure in Scheme 1 furnished **10b** as white solid. Yield: 9.84%, mp 173.5-177.7℃, HPLC: 95.88%. ^{1}H NMR (500 MHz, DMSO-d_6): δ9.34 (d, J = 9.2 Hz, 1H), 9.06 (d, J = 7.8 Hz, 1H), 8.61 (s, 1H), 8.51 (s, 1H), 8.48–8.43 (m, 2H), 8.39–8.31 (m, 1H), 7.66 (s, 2H), 7.29 (d, J = 7.3 Hz, 2H), 7.19 (d, J = 4.4 Hz, 4H), 4.42 (dd, J = 8.0, 5.7 Hz, 4H), 3.04 (d, J = 7.7 Hz, 4H). ^{13}C NMR (126 MHz, DMSO-d_6): δ158.09 (d, J = 12.8 Hz), 156.30 (s), 155.89 (s), 155.31 (s), 149.51 (d, J = 5.0 Hz), 136.89 (s), 134.91 (s), 123.91 (d, J = 6.1 Hz), 122.14 (s), 101.65 (s), 100.39 (s), 99.39 (s), 71.92 (s), 68.88 (s), 64.88 (s), 64.50 (s), 37.27 (d, J = 11.4 Hz). HRMS (ESI) m/z calcd for $[C_{25}H_{23}C_{l6}N_9O_4+H]^+$: 724.0077, found: 724.0083.

2-(pyridin-2-yl) ethyl (2,2,2-trichloro-1-(4-hydroxy-1H-pyrazolo[3,4-d]pyrimidin-1-yl)ethyl) carbamate (10c) Following general procedure in Scheme 1 furnished **10c** as colorless solid. Yield: 7.22%, mp 138.7-140.8℃, HPLC: 95.06%. 1H NMR (500 MHz, DMSO-d_6): δ12.49 (s, 1H), 9.41 (d, J = 9.6 Hz, 1H), 8.46 (s, 1H), 8.28 (s, 1H), 8.22 (s, 1H), 7.68 (t, J = 6.7 Hz, 1H), 7.31 (d, J = 7.0 Hz, 1H), 7.25-7.19 (m, 1H), 7.12 (d, J = 9.8 Hz, 1H), 4.42 (dd, J = 13.4, 6.5 Hz, 2H), 3.05 (t, J = 6.3 Hz, 2H). ^{13}C NMR (126 MHz, DMSO-d_6): δ157.99 (s), 157.44 (s), 154.15 (s), 149.73 (s), 149.45 (s), 137.04 (s), 136.81 (s), 124.05 (s), 122.17 (s), 116.17 (s), 106.07 (s), 99.15 (s), 72.11 (s), 64.92 (s), 37.14 (s). HRMS (ESI) m/z calcd for $[C_{15}H_{13}Cl_3N_6O_3+H]^+$: 431.0187, found: 431.0193.

Cell Culture and Cytotoxicity Assay All cells were cultured according to the supplier's instructions. Briefly, liver hepatocellular cells (HepG2) and human ovarian cancer cells (OVCAR-3 and Caov-3) were grown in DMEM (Gibco) containing 4.5 g/L glucose supplemented with 10% FBS and 1% glutamine. Human non-small-cell lung carcinoma cells (A549), human cervix carcinoma cells (Hela), human malignant melanoma cells (A375), and human breast adenocarcinoma cells (MCF-7) were grown in RPMI 1640 (Gibco) containing 10% FBS and 1% glutamine. All cell lines were purchased from the Xiangya Cell Bank, Central South University, Changsha, China and incubated at 37℃ with 5% CO_2 in a humidified atmosphere. Cytotoxicity assay was assessed using 3-(4,5-dimethyl-2-thiazolyl)-2,5-diphenyl-2H-tetrazolium bromide (MTT) according to the manufacturer's instructions. Cells were seeded in triplicate into 96-well plates (4-5×10^3cells/well, 100 μL) and allowed to adhere overnight. Cells were incubated with test compounds at concentrations ranging from 0.03 to 300 μM (DMSO less than 0.1% in each preparation) for 48 h. Thereafter, 10 μL of MTT (5 mg/mL) was added, and the cells were incubated at 37°C for another 4 h. The reduced MTT crystals were dissolved in 150 μL of DMSO, and the absorbance was measured by a microplate reader (Bio-Tek, Cytation™ 5 Cell Imaging Multi-Mode Reader, USA). The anti-proliferative effect of compound was expressed as IC_{50} value. Experiments were performed in triplicate.

SPR Analysis SPR is used to measure bio-molecular interactions without labeling. Surface plasmon resonance data were collected on an OpenSPRTM system. For OpenSPRTM data, the binding of compounds to Cdc20 protein was monitored with the OpenSPRTM system. The acid-coupling chip was installed according to the OpenSPRTM standard operating procedures and then phosphate buffered saline (PBS, pH 7.4) was run at a maximum flow rate of 150uL/min. After reaching the baseline of the signal, 200 μL of 80% isopropanol (IPA) was loaded and run

for 10 s to remove bubbles. After reaching the baseline, the sample loop was washed with buffer and evacuated with air. Binding studies were performed at a constant flow rate of 20μL/min in instrument running buffer until the signal reached the baseline. Thereafter, 200 μL of 1-ethyl-3-(3-(dimethylamino)propyl) carbodiimide hydrochloride (EDC)/N-hydroxy succinimide (NHS) solution was loaded, and the sample loop was washed with buffer and evacuated with air. The purified protein Cdc20 was diluted with buffer, injected, and run for 4 min, followed by injection of 200 μL of blocking solution, washing the sample loop with buffer, and evacuation with air. SPR binding data were obtained using an appropriate gradient dilution series for each compound and injected as the running buffer. Small molecules were injected consecutively for 120-140 s association, and the natural dissociation time was 160 s. The affinity parameters were evaluated in a steady state One To One analysis model using the TraceDrawer (Ridgeview Instruments ab, Sweden). The purity of CDC20 (Human) Recombinant Protein (Abnova, P01) was over 95%.

Molecular Modeling The crystal structure of tubulin in complex with different ligands was downloaded from PDB (http://www.rcsb.org/; PDB codes 4n14, 2R75, 5NJH and 5OSK). Missing hydrogen atoms in the crystal structure were computationally added and proteins were preprocessed by 3 d protonation, Mg^{2+}, GDP, GTP, and all the other bound small molecules, except the target ligand, were deleted. Ligand structures were built with MOE.2014 and minimized using the MMFF94x force field. The ligands were then prepared to generate low-energy ring conformers. Molecular docking was performed using MOE for the ability of molecules to bind the ligand sites.

Immunofluorescence HepG2 cells were seeded at a density of 4×10^3 cells/well in Costar 96-well plates and incubated overnight to adhere. Cells were then treated with different concentrations of compounds. After 48 h of treatment with the compounds, cells were fixed with

4% formaldehyde for 15 min at room temperature, and then the fixative was decanted. The wells were washed three times with 100 μL of PBS for 15 min. The PBS was subsequently aspirated, and the cells were permeabilized by addition of 100 μL of Triton X-100 for 15 min. The Triton X-100 was aspirated, and the wells were washed three times with 100 μL of PBS for 15 min and BSA was added for 15 min to block nonspecific binding sites. The cells were incubated with anti-phospho-histone H3 (Cell Signaling, #9701) and anti-α-tubulin (Cell Signaling, #2144) at 4 ℃ overnight, followed by washing with PBS. After washing, the cells were treated with secondary antibodies (Alex Fluor®-labeled anti-rabbit IgG for α-tubulin and phospho-histone H3) and then counterstained with DAPI (Beyotime, C1002). Analysis was carried out using the Gen 3.04 instrument to measure cellular levels of phosphohistone H3 and α-tubulin.

Western Blot Analysis Protein extracts of cells were prepared by lysis in radioimmunoprecipitation assay buffer (Sigma) containing protease and phosphatase inhibitors (Complete protease inhibitor cocktail, Roche). Protein extracts (25 μg) were separated by SDS-PAGE and transferred onto polyvinylidene fluoride membranes using the TransBlot Turbo Transfer System (BioRad). After blocking with 5% skim milk powder in TBST for 1 h, the whole PVDF membrane was cut into required pieces according to the protein marker and expected molecular weight. These pieces were incubated overnight at 4℃with corresponding primary antibodies against Cyclin A2, Cyclin B1, Cleaved PARP (Cell Signaling Technology, Beverly, MA, USA), Aurora A, Skp2, and Bim (Beyotime). Afterwards, these pieces were washed three times with TBST buffer, and then incubated with a secondary antibody conjugated with HRP for 1 h at room temperature, followed by ECL detection (ECL Chemiluminescent Western Blot Substrate, Pierce). Each piece was detected separately. The representative blots were shown in the figures and quantified by ImageJ. The results were shown as histograms.

In Vitro Tubulin Polymerization Assay The fluorescence-based in vitro tubulin polymerization assay was performed using the Tubulin Polymerization Assay Kit (BK004P, Cytoskeleton, USA) according to the instruction. Various concentrations of test compounds were preplated at 10× final assay concentration (10 μL/well), and then a solution of porcin brain tubulin (4 mg/mL) in G-PEM buffer (80 mM PIPES pH 6.9, 2 mM $MgCl_2$, 0.5 mM EGTA) was prepared freshly on ice and promptly distributed into the reaction wells at 100 μL/well. Immediately, the assembly kinetics of tubulin was monitored at OD_{340} at 30 s intervals (37°C) over 60 min using the Gen 3.04 multimode reader. Data from each well were normalized relative to initial readings, and plots of ΔOD_{max} (final−initial values) against compound concentration, expressed relative to vehicle control (DMSO only), were used to calculate IC_{50} values.

Cell Apoptosis Assay Cells were seeded at a density of 4×10^4 cells/well in 24-well plates and treated with different concentrations of compounds. After 24 h, cells were harvested and washed with PBS. Cells were stained with 2 μL of FITC-conjugated anti-Annexin V antibody and 2 μL of PI (propidium iodide) diluted in 200 μL of binding buffer, and then analyzed with a microplate reader (A211-02, Vazyme) and Flow Cytometer (ACEA NovoCyte™).

Wound Healing Assays HepG2 cells were seeded in 24-well plates overnight (15×10^4 cells/well) in replicates of three. Scratches were made in confluent monolayers using 10 μL microtips. Thereafter, the wounds were washed three times with PBS to remove any debris and uprooted cells. The media containing 0.3 μM of **9f** was added to the Petri dishes. Cells which migrated across the wound area were photographed using the microplate reader (Bio-Tek, Cytation 5) at 0, 24, 48, and 72 h. The reproducibility of the results was confirmed by at least two separate experiments. Images were captured and the wound area was measured with ImageJ software (NIH, Bethesda, MD).

Cell Invasion Assay Cells treated with **9f** and DMSO were seeded in the upper chamber (Corning, NY, USA) with 200 μL of serum-free medium with Matrigel (BD Biosciences, San Jose, CA), and 600 μL of complete medium was added to the lower chamber. After incubation for 48 h at 37℃ with 5% CO_2, the invasive cells were stained with crystal violet and photographed with microscope. The reproducibility of the results was confirmed by at least two separate experiments.

Statistical Analysis For data analysis and graphic presentation, the nonlinear multipurpose curve-fitting GraphPad Prism (GraphPad) 7.0 software package was used. $P < 0.05$ was considered as statistically significant.

■ ASSOCIATED CONTENT

Supporting Information

The Supporting Information is available free of charge on the ACS Publications website at DOI:

Ligand interactions of molecule-cdc20 complex and molecule-microtubule complex, Images captured at 0, 6, 18, 24, 40, 48h after cells were treated with 0.3 μM of **9f**. SPR result of **8g**. HPLC, HRMS, ^{1}H NMR, and ^{13}C NMR of target compounds. Quantitative results of Western Blot. (PDF)

Docking Models. (PDB)

Molecular formula strings and biological data. (CSV)

■ AUTHOR INFORMATION

Corresponding Author

*E-mail: cz_job@csu.edu.cn. Phone: +86-0731-82650370. Fax: +86-0371-82650370.

Author Contributions

#Pan Huang and Xiangyang Le comtributed equally.

Notes

Most of the target compounds that reported in this manuscript were synthesized by Xiangyang Le, and Xiangyang Le had no contribution to biological research design, data collections, data analyses, or the writing of this manuscript. The authors declare no competing financial interest.

■ ACKNOWLEDGMENT

This work was supported by the National Natural Science Foundation of China (No. 81573287 & 81773640) and Postgraduates innovation subject of Central South University (No. 2018zzts867). Additional support was from the Nuclear Magnetic Resonance Laboratory of Advanced Research Center in Central South University for NMR spectra analysis.

■ ABBREVIATIONS

Cdc20, Cell Division Cycle 20 Homologue; SPR, surface plasmon resonance; E1, ubiquitin-activating enzyme; E2, ubiquitin-conjugating enzyme; E3, ubiquitin-ligase enzyme; APC/C, anaphase-promoting complex/cyclosome; Cdh1, Cdc20 homologue protein 1, Fzr1; SAC, spindle assembly checkpoint; PPI, protein-protein interactions; MIA, microtubule interfering agent; K_D, binding affinity; PI, propidium iodide; MTT, 3-(4,5-dimethyl-2-thiazolyl)-2,5-diphenyl-2H-tetrazolium bromide.

■ REFERENCES

(1) Bassermann, F.; Eichner, R.; Pagano, M. The Ubiquitin Proteasome System-Implications for Cell Cycle Control and the Targeted Treatment of Cancer. *Biochim. Biophys. Acta* **2014**, *1843*, 150-162.

(2) Zhou, Z.; He, M.; Shah, A. A.; Wan, Y. Insights into APC/C: From Cellular Function to Diseases and Therapeutics. *Cell Div.* **2016**, *11*, 9, doi: 10.1186/s13008-016-0021-6.

(3) Davey, N. E.; Morgan, D. O. Building a Regulatory Network with Short Linear Sequence Motifs: Lessons from the Degrons of the Anaphase-Promoting Complex. *Molecular cell* **2016**, *64(1)*, 12–23.

(4) Sivakumar, S.; Gorbsky, G. J. Spatiotemporal Regulation of the Anaphase-Promoting Complex in Mitosis. *Nat. Rev. Mol. Cell Biol*. **2015**, *16*, 82-94.

(5) Zhang, J.; Wan, L.; Dai, X.; Sun, Y.; Wei, W. Functional Characterization of Anaphase Promoting Complex/Cyclosome (APC/C) E3 Ubiquitin Ligases in Tumorigenesis. *Biochim. Biophys. Acta* **2014**, *1845*, 277-293.

(6) Fujita, T.; Liu, W.; Doihara, H.; Wan, Y. An in vivo Study of Cdh1/APC in Breast Cancer Formation. *Int. J. Cancer* **2009**, *125*, 826-836.

(7) Fujita, T.; Liu, W.; Doihara, H.; Date, H.; Wan, Y. Dissection of the APC^{Cdh1}-Skp2 Cascade in Breast Cancer. *Clin. Cancer Res*. **2008**, *14*, 1966-1975.

(8) Qiao, X.; Zhang, L.; Gamper, A. M.; Fujita, T.; Wan, Y. APC/C-Cdh1: From Cell Cycle to Cellular Differentiation and Genomic Integrity. *Cell Cycle* **2010**, *9*, 3904-3912.

(9) Wang, L.; Zhang, J.; Wan, L.; Zhou, X.; Wang, Z.; Wei, W. Targeting Cdc20 as A Novel Cancer Therapeutic Strategy. *Pharmacol. Ther*. **2015**, *151*, 141-151.

(10) Shang, G.; Ma, X.; Lv, G. Cell Division Cycle 20 Promotes Cell Proliferation and Invasion and Inhibits Apoptosis in Osteosarcoma Cells. *Cell Cycle* **2018**, *17*, 43-52.

(11) Karra, H.; Repo, H.; Ahonen, I.; Loyttyniemi, E.; Pitkanen, R.; Lintunen, M.; Kuopio, T.; Soderstrom, M.; Kronqvist, P. Cdc20 and Securin Overexpression Predict Short-term Breast Cancer Survival. *Br. J. Cancer* **2014**, *110*, 2905-2913.

(12) Wu, W. J.; Hu, K. S.; Wang, D. S.; Zeng, Z. L.; Zhang, D. S.; Chen, D. L.; Bai, L.; Xu, R. H. CDC20 Overexpression Predicts a Poor Prognosis for Patients with Colorectal Cancer. *J. Transl. Med*. **2013**, *11*, 142, doi: 10.1186/1479-5876-11-142.

(13) Wang, J.; Zhou, F.; Li, Y.; Li, Q.; Wu, Z.; Yu, L.; Yuan, F.; Liu, J.; Tian, Y.; Cao, Y.; Zhao, Y.; Zheng, Y. Cdc20 Overexpression is Involved in Temozolomide-resistant Glioma Cells with Epithelial-mesenchymal Transition. *Cell Cycle* **2017**, *16*, 2355-2365.

(14) Ding, Y.; Yu, S.; Bao, Z.; Liu, Y.; Liang, T. CDC20 with Malignant Progression and Poor Prognosis of Astrocytoma Revealed by Analysis on Gene Expression. *J. Neurooncol*. **2017**, *133*, 87-95.

(15) Regenbrecht, C. R.; Jung, M.; Lehrach, H.; Adjaye, J. The Molecular Basis of Genistein-Induced Mitotic Arrest and Exit of Self-renewal in Embryonal Carcinoma and Primary Cancer Cell Lines. *BMC. Med. Genomics* **2008**, *1*, 49, doi: 10.1186/1755-8794-1-49.

(16) Das, T.; Roy, K. S.; Chakrabarti, T.; Mukhopadhyay, S.; Roychoudhury, S. Withaferin A Modulates the Spindle Assembly Checkpoint by Degradation of Mad2-Cdc20 Complex in Colorectal Cancer Cell Lines. *Biochem. Pharmacol*. **2014**, *91*, 31-39.

(17) Nasr, T.; Bondock, S.; Youns, M. Anticancer Activity of New Coumarin Substituted Hydrazide-Hydrazone Derivatives. *Eur. J. Med. Chem*. **2014**, *76*, 539-548.

(18) Zhang, Y.; Xue, Y. B.; Li, H.; Qiu, D.; Wang, Z. W.; Tan, S. S. Inhibition of Cell Survival by Curcumin Is Associated with Downregulation of Cell Division Cycle 20 (Cdc20) in Pancreatic Cancer Cells. *Nutrients* **2017**, *9*, 109, doi: 10.3390/nu9020109.

(19) Jiang, J.; Jedinak, A.; Sliva, D. Ganodermanontriol (GDNT) Exerts Its Effect on Growth and Invasiveness of Breast Cancer Cells through the Down-regulation of CDC20 and uPA. *Biochem. Biophys. Res. Commun*. **2011**, *415*, 325-329.

(20) Jiang, J.; Thyagarajan-Sahu, A.; Krchnak, V.; Jedinak, A.; Sandusky, G. E.; Sliva, D. NAHA, a Novel Hydroxamic Acid-Derivative, Inhibits Growth and Angiogenesis of Breast Cancer in vitro and in vivo. *PLoS One* **2012**, *7*, e34283, doi: 10.1371/journal.pone.0034283.

(21) Zeng, X.; Sigoillot, F.; Gaur, S.; Choi, S.; Pfaff, K. L.; Oh, D. C.; Hathaway, N.; Dimova, N.; Cuny, G. D.; King, R. W. Pharmacologic Inhibition of the Anaphase-Promoting Complex Induces a Spindle Checkpoint-Dependent Mitotic Arrest in the Absence of Spindle Damage. *Cancer cell* **2010**, *18*, 382–395.

(22) Sackton, K. L.; Dimova, N.; Zeng, X.; Tian, W.; Zhang, M.; Sackton, T. B.; Meaders, J.; Pfaff, K. L.; Sigoillot, F.; Yu, H.; Luo, X.; King, R. W. Synergistic Blockade of Mitotic Exit by Two Chemical Inhibitors of the APC/C. *Nature* **2014**, *514*, 646–649.

(23) Raab, M.; Sanhaji, M.; Zhou, S.; Rödel, F.; El-Balat, A.; Becker, S.; Strebhardt, K. Blocking Mitotic Exit of Ovarian Cancer Cells by Pharmaceutical Inhibition of the Anaphase-Promoting Complex Reduces Chromosomal Instability. *Neoplasia* **2019**, *21*, 363–375.

(24) Raab, M.; Kobayashi, N. F.; Becker, S.; Kurunci-Csacsko, E.; Krämer, A.; Strebhardt, K.; Sanhaji, M.; Boosting the Apoptotic Response of High-Grade Serous Ovarian Cancers with CCNE1 Amplification to Paclitaxel in vitro by Targeting APC/C and the Pro-survival Protein MCL-1. *Int. J. Cancer* **2020**, *146*, 1086-1098.

(25) Mills, C. C.; Kolb, E. A.; Sampson, V. B. Recent Advances of Cell-Cycle Inhibitor Therapies for Pediatric Cancer. *Cancer Res*. **2017**, *77*, 6489-6498.

(26) Casaluce, F.; Sgambato, A.; Maione, P.; Ciardiello, F.; Gridelli, C. Emerging Mitotic Inhibitors for Non-small Cell Carcinoma. *Expert Opin. Emerg. Drugs* **2013**, *18*, 97-107.

(27) Kaur, R.; Kaur, G.; Gill, R. K.; Soni, R.; Bariwal, J. Recent Developments in Tubulin Polymerization Inhibitors: An Overview. *Eur. J. Med. Chem*. **2014**, *87*, 89-124.

(28) Haider, K.; Rahaman, S.; Yar, M. S.; Kamal, A. Tubulin Inhibitors as Novel Anticancer Agents: An Overview on Patents (2013-2018). *Expert Opin. Ther. Pat*. **2019**, *29*, 623-641.

(29) Smolders, L.; Teodoro, J. G.; Targeting the Anaphase Promoting Complex: Common Pathways for Viral Infection and Cancer Therapy. *Expert Opin. Ther. Targets* **2011**, *15*, 767-780.

(30) Manchado, E.; Guillamot, M.; Malumbres, M. Killing Cells by Targeting Mitosis. *Cell Death Differ*. **2012**, *19*, 369-377.

(31) Penna, L. S.; Henriques, J.; Bonatto, D. Anti-mitotic agents: Are They Emerging Molecules for Cancer Treatment? *Pharmacol. Ther*. **2017**, *173*, 67-82.

(32) Wan, L.; Tan, M.; Yang, J.; Inuzuka, H.; Dai, X.; Wu, T.; Liu, J.; Shaik, S.; Chen, G.; Deng, J.; Malumbres, M.; Letai, A.; Kirschner, M. W.; Sun, Y.; Wei, W. APC(Cdc20) Suppresses Apoptosis through Targeting Bim for Ubiquitination and Destruction. *Dev. Cell* **2014**, *29*, 377-391.

(33) Wang, Q.; Arnst, K. E.; Wang, Y.; Kumar, G.; Ma, D.; White, S. W.; Miller, D. D.; Li, W.; Li, W. Structure-Guided Design, Synthesis, and Biological Evaluation of (2-(1H-Indol-3-yl)-1H-imidazol-4-yl)(3,4,5-trimethoxyphenyl)Methanone (ABI-231) Analogues Targeting the Colchicine Binding Site in Tubulin. *J. Med. Chem*. **2019**, *62* , 6734-6750.

(34) Nakaqawa-Goto, K.; Oda, A.; Hamel, E.; Ohkoshi, E.; Lee, K. H.; Goto, M. Development of a Novel Class of Tubulin Inhibitor from Desmosdumotin B with a Hydroxylated Bicyclic B-Ring. *J. Med. Chem*. **2015**, *58*, 2378-2389.

(35) Li, W.; Sun, H.; Xu, S.; Zhu, Z.; Xu, J. Tubulin Inhibitors Targeting the Colchicine Binding Site: A Perspective of Privileged Structures. *Future Med. Chem*. **2017**, *9*, 1765-1794.

(36) Dong, M.; Liu, F.; Zhou, H.; Zhai, S.; Yan, B. Novel Natural Product- and Privileged Scaffold-Based Tubulin Inhibitors Targeting the Colchicine Binding Site. *Molecules* **2016**, *21*, 1375, doi:10.3390/molecules21101375.

(37) Dohle, W.; Jourdan, F. L.; Menchon, G.; Prota, A. E.; Foster, P. A.; Mannion, P.; Hamel, E.; Thomas, M. P.; Kasprzyk, P. G.; Ferrandis, E.; Steinmetz, M. O.; Leese, M. P.; Potter, B. Quinazolinone-Based Anticancer Agents: Synthesis, Antiproliferative SAR, Antitubulin Activity, and Tubulin Co-crystal Structure. *J. Med. Chem*. **2018**, *61*, 1031-1044.

(38) Zhou, Z. Z.; Shi, X. D.; Feng, H. F.; Cheng, Y. F.; Wang, H. T.; Xu, J. P. Discovery of 9H-Purins as Potential Tubulin Polymerization Inhibitors: Synthesis, Biological Evaluation and Structure-Activity Relationships. *Eur. J. Med. Chem*. **2017**, *138*, 1126-1134.

(39) Kapanidou, M.; Curtis, N. L.; Bolanos-Garcia, V. M. Cdc20: At the Crossroads between Chromosome Segregation and Mitotic Exit. *Trends Biochem. Sci*. **2017**, *42*, 193-205.

(40) Wang, Z.; Wan, L.; Zhong, J.; Inuzuka, H.; Liu, P.; Sarkar, F. H.; Wei, W. Cdc20: A Potential Novel Therapeutic Target for Cancer Treatment. *Curr. Pharm. Des*. **2013**, *19*, 3210-3214.

Table of Contents graphic

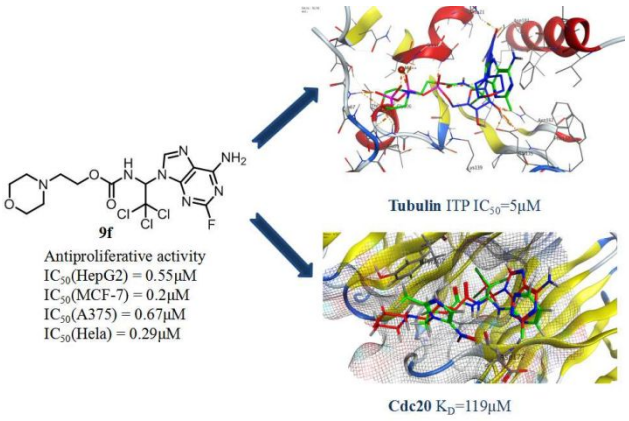

A series of 2,2,2-trichloro-1-aryl carbamate derivatives generated from the structural modification of the apcin were designed and synthesized. The most potent compound **9f** showed excellent in vitro antitumor activity due to its dual inhibition of tubulin polymerization and Cdc20.